GLOBULAR CLUSTER ABUNDANCES FROM HIGH-RESOLUTION, INTEGRATED-LIGHT SPECTROSCOPY. III. THE LARGE MAGELLANIC CLOUD: FE AND AGES[1]

Janet E. Colucci
Department of Astronomy and Astrophysics, 1156 High Street, UCO/Lick Observatory,
University of California, Santa Cruz, CA 95064; jcolucci@ucolick.org

Rebecca A. Bernstein
Department of Astronomy and Astrophysics, 1156 High Street, UCO/Lick Observatory,
University of California, Santa Cruz, CA 95064; rab@ucolick.org

Scott A. Cameron
Science Department, 3000 College Heights Blvd., Cerro Coso Community College, Ridgecrest, CA 93555; scameron@cerrocoso.edu

and

Andrew McWilliam
The Observatories of the Carnegie Institute of Washington, 813 Santa Barbara Street, Pasadena, CA 91101-1292; andy@ociw.edu
Submitted October 17, 2010, Accepted January 19, 2013

ABSTRACT

In this paper we refine our method for the abundance analysis of high resolution spectroscopy of the integrated light of unresolved globular clusters (GCs). This method was previously demonstrated for the analysis of old (>10 Gyr) Milky Way GCs. Here we extend the technique to young clusters using a training set of 9 GCs in the Large Magellanic Cloud (LMC). Depending on the signal-to-noise ratio of the data, we use 20-100 Fe lines per cluster to successfully constrain the ages of old clusters to within a ∼5 Gyr range, the ages of ∼2 Gyr clusters to a 1-2 Gyr range, and the ages of the youngest clusters (0.05-1 Gyr) to a ∼200 Myr range. We also demonstrate that we can measure [Fe/H] in clusters with any age less than 12 Gyrs with similar or only slightly larger uncertainties (0.1-0.25 dex) than those obtained for old Milky Way GCs (0.1 dex); the slightly larger uncertainties are due to the rapid evolution in stellar populations at these ages. In this paper, we present only Fe abundances and ages. In the next paper in this series, we present our complete analysis of the ∼ 20 elements for which we are able to measure abundances. For several of the clusters in this sample, there are no high resolution abundances in the literature from individual member stars; our results are the first detailed chemical abundances available. The spectra used in this paper were obtained at Las Campanas with the echelle on the du Pont Telescope and with the MIKE spectrograph on the Magellan Clay Telescope.

Subject headings: galaxies: individual (LMC) — galaxies: star clusters — galaxies: abundances — globular clusters: individual(NGC 2005, NGC 2019, NGC 1916, NGC 1978, NGC 1718, NGC 1866, NGC 1711, NGC 2100, NGC 2002) — stars: abundances

1. INTRODUCTION

Globular clusters (GCs) are unique tools for probing the formation history and evolution of galaxies. The ∼150 GCs (Harris 1996) of the Milky Way (MW) have been studied extensively and have provided fundamental clues to our current picture of the formation of the MW, and by extension, other normal spiral galaxies. Particularly interesting constraints have come from detailed chemical abundances of individual member stars in the MW GCs, which show relative abundance patterns that can be used to constrain the early star formation history of the MW.

Because GCs are so luminous, extragalactic GCs can also be individually identified and studied as unresolved sources. Because they are spatially unresolved, however, extragalactic GC systems have typically been studied with low resolution spectroscopy and photometry. Detailed abundance work requires high resolution, high

signal-to-noise ratio (S/N) spectra and so has been done solely on individual, resolved stars in the past, which limited such studies to stars in the MW and nearby dwarf galaxies. In order to measure detailed chemical abundances of stellar systems beyond the MW, we have developed a new technique for analyzing high resolution spectra of the integrated light (IL) of GCs. With this technique, we can measure both ages and detailed chemical abundances of ∼20 elements in a moderate quality (S/N∼50), high resolution ($R \equiv \lambda/\Delta\lambda \sim 20,000$) spectrum of a typical GC. Our technique now allows us to study the chemical evolutionary history of distant galaxies at an unprecedented level of detail that has previously only been possible within the MW. We can now begin to constrain the star formation rate (SFR), stellar initial mass function (IMF), gas inflow/outflow, and chemical evolution history of galaxies within roughly 4 Mpc, well beyond the nearest neighbors of the MW.

Previous techniques utilizing IL spectra of unresolved, extragalactic clusters focused on estimating metallicities (e.g. [Fe/H]) and α-element abundance ratios from low

[1] This paper includes data gathered with the 6.5 meter Magellan Telescopes located at Las Campanas Observatory, Chile.

Table 1
LMC Cluster Sample

Cluster	RA (2000)	Dec (2000)	V[a]	$B-V$	$E(B-V)$	Age (Gyrs)	[Fe/H]	$[\alpha/\text{Fe}]$[b]	References[c]
Old (> 5 Gyrs)									
NGC 1916	5 18 37.9	−69 24 23	10.38	0.78±0.02	0.13±0.02	>10	−2.08	···	1,13
NGC 2019	5 31 56.5	−70 09 32	10.95	0.77±0.01	0.06±0.02	>10	−1.37	+0.20	2, 14
NGC 2005	5 30 10.4	−69 45 09	11.57	0.73	0.10±0.02	>10	−1.80	+0.05	2, 14
Intermediate Age (1-3 Gyrs)									
NGC 1978	5 28 45.0	−66 14 14	10.74	0.78±0.04	0.09	1.9	−0.38	+0.02	3,7
							−0.96	+0.38	4
NGC 1718	4 52 25.0	−67 03 06	12.25	0.76±0.01	0.10±0.03	2.1	−0.80	···	5,6
Young (< 1 Gyr)									
NGC 1866	5 13 38.9	−65 27 52	9.89	0.26±0.02	0.06	0.13	−0.51	+0.08	4,15
							−0.43	+0.00	16
NGC 1711	4 50 37.0	−69 59 06	10.11	0.20±0.08	0.09±0.05	0.050	−0.57	···	8
NGC 2002	5 30 21.0	−66 53 02	10.1	0.00	0.20	0.018	−2.2	···	11, 12
NGC 2100	5 42 08.6	−69 12 44	9.60	0.16±0.02	0.26±0.01	0.015	−0.32	−0.06	9, 10, 13

[a] From Pessev et al. (2008) and Bica et al. (1996)
[b] Mean of [Si/Fe], [Ca/Fe], and [Ti/Fe] abundances from 2, 3, 9, and 16 and mean of [O/Fe] from 4.
[c] References for columns 4, 5, 6 and 7: 1.Olszewski et al. (1991), 2. Johnson et al. (2006), 3. Mucciarelli et al. (2008), 4. Hill et al. (2000), 5. Grocholski et al. (2006), 6. Kerber et al. (2007), 7. Mucciarelli et al. (2007), 8. Dirsch et al. (2000), 9. Jasniewicz & Thevenin (1994), 10. Elson (1991), 11. Kumar et al. (2008), 12. Wolf et al. (2007), 13. Pessev et al. (2008), 14. Olsen et al. (1998),15. Walker et al. (2001), 16. Mucciarelli et al. (2010)

resolution spectra with line index systems like the "Lick" system (e.g. Faber et al. 1985). While very useful for obtaining information on the general chemical properties of GC systems, line indexes are inaccurate, and even state of the art line index or full spectrum fitting techniques for lower resolution will always be limited to measurements of at most ∼ 5 elements (e.g. Graves & Schiavon 2008). In fact, line index systems were originally designed to target unresolved galaxies in which spectral lines of individual elements are not possible to resolve due to the high internal velocity dispersions $(100-300 \, \text{km s}^{-1})$ of the galaxies themselves (e.g. Faber & Jackson 1976). GCs, on the other hand, have small velocity dispersions of $2-25 \, \text{km s}^{-1}$, so that weak lines are not blended and broadened; features of many elements are easily identifiable in spectra of their integrated light. The availability of over 20 individual elements makes our method particularly powerful for chemical evolution studies compared to low and medium resolution (see new "LIS" system of Vazdekis et al. 2010) line index methods.

Our IL abundance analysis technique relies on the fact that GCs are SSPs, and thus can be easily modeled (Bernstein et al. 2003; Bernstein & McWilliam 2002, 2005; McWilliam & Bernstein 2008). Unlike line index systems (see Puzia et al. 2002), this method is based on explicit measurements of individual absorption features and is analogous to standard analyses of red giant branch (RGB) stars. Thus, our abundance analysis does not rely on a calibration to local MW stars, and there are no systematic errors due to built in assumptions on the chemical nature of the target clusters. Briefly, our IL abundance analysis utilizes the fact that stellar evolution is reasonably well understood (e.g. Gallart et al.

2005), so that it is straightforward to use theoretical stellar isochrones to create arbitrary synthetic stellar populations of bound star clusters that are characterized only by their age and metallicity. These synthetic GC populations can then be used to synthesize flux-weighted, IL spectra for comparison to the observed IL spectra of unresolved GCs. Of course there are some aspects of stellar evolution that are not perfectly produced in the isochrones. For example, it is well known that the properties of blue horizontal branch stars are not accurately produced from first principles and that parameters such as mass loss must be adjusted to match observations (e.g. Pietrinferni et al. 2004). Other sources of uncertainty in the isochrones include fractional contributions from blue stragglers, asymptotic giant branch stars, and young supergiants. Fortunately, the presence of these types of stars can be inferred from our spectra themselves. We discuss several of the potential diagnostic tools for evaluating the more uncertain phases of stellar evolution and their impact on our analysis in this paper.

While we do so in a integrated light spectrum, our IL abundance analysis technique utilizes the same standard stellar high resolution abundance analysis methods that have been in use for decades; we use equivalent widths (EWs) and line profile fitting of individual spectral features and spectral line synthesis to derive abundances. Clean, unblended features with well determined transition strengths can be readily measured in our spectra, and the self-consistency and stability of the abundance solution for many (50-150) individual transitions of Fe can be used to constrain the best-fitting synthetic GC population. Using the stability of the Fe line solutions, the most appropriate stellar population (characterized

by its age and abundance) can be matched to any unresolved GC using the observed IL spectra alone. This best-fitting stellar population can then be used to derive abundances of ∼20 different chemical elements.

In McWilliam & Bernstein (2008) (hereafter Paper I), Bernstein et al. (2011a, in preparation) (hereafter Paper II), Cameron (2009) and Colucci (2010), extensive testing on a "training set" of MW GCs of known properties was presented with the development of our IL abundance analysis method. These works focused on demonstrating the analysis method and the accuracy of the derived abundances for a set of "typical" MW GCs, which have old ages (>10 Gyr), span a range in metallicity from [Fe/H]∼ −2 to −0.4, and have a spread in horizontal branch morphology and internal velocity dispersion (σ_V). The results of Paper I and Paper II showed that the abundances measured using our IL analysis method have accuracies of ≤0.1 dex for nearly all species when compared to standard analysis of individual stars in the training set clusters, and that the statistical uncertainties in abundances for individual element species are ∼0.2 dex, which is comparable to the precision in abundance measurements in those GCs obtained from single member RGB stars (≲0.15 dex). For old GCs, ages can be constrained to a range of 5 Gyr, which is small enough that the adopted age affects the abundance results by <0.1 dex, which is less than the statistical error of the measured spectral lines.

In this paper, the third of the series, we have two primary goals. The first is to demonstrate that the IL abundance analysis method can be applied to clusters younger than 10 Gyr in age. Because there are few, if any, high mass, high surface brightness young star clusters in the MW, we have used clusters in the Large Magellanic Cloud (LMC) for this purpose. Although most young clusters are not massive enough to survive a Hubble time, they are still valuable tools for studying the chemical evolution of galaxies as a function of time. As part of further developing the IL method for young clusters, we also present an additional technique for evaluating the effect of stochastic stellar population fluctuations on the measurement of age and [Fe/H] of unresolved clusters. Our second goal in this work is to measure new detailed chemical abundances for LMC clusters that have not been previously studied with high resolution spectroscopy. In this paper we present new results for [Fe/H] in three, previously unstudied clusters; results for approximately 20 additional elements in each cluster are presented in a following paper Colucci et al. (2011b, in preparation), hereafter "Paper IV."

The properties of the LMC training set clusters are discussed in detail in § 2 . In § 3 we discuss the observations and data reduction, and in § 4 we describe our analysis techniques as well as age and [Fe/H] results for each cluster. In § 5 we compare the IL abundances for the training set clusters to previous work using high resolution spectra of individual stars, and to results from photometry and low resolution spectra. We also discuss the age-metallicity relation we have found for the LMC clusters in this work.

2. GLOBULAR CLUSTER TRAINING SET

The goals of this paper and Paper IV are to refine the integrated light method developed in Paper I and Paper II on clusters in the LMC, and also to measure new abundances for LMC clusters previously unstudied at high resolution. To this end, it is important to consider differences between the LMC training set and the MW training set along with the limitations of the LMC training set when compared to distant, unresolved clusters. Overall, the LMC training set data is unavoidably of lower quality (i.e. lower S/N) than the data obtained for the MW training set because the clusters are generally less massive, and therefore less luminous, and they lie at much greater distances (D∼50 kpc). This makes the LMC training set data useful to evaluate the accuracy of the IL method when applied to lower S/N data of distant, unresolved clusters.

Our training set includes seven MW clusters, as described in Paper I and Paper II, as well as nine LMC clusters (NGC 1916, NGC 2005, NGC 2019, NGC 1978, NGC 1718, NGC 1866, NGC 1711, NGC 2100, and NGC 2002). The LMC training set includes clusters <10 Gyr old, which is an age range that cannot be probed using clusters in the MW alone. In addition, the LMC training set provides old clusters with a range of abundance ratios (Johnson et al. 2006). This is in contrast to MW clusters, which have very uniform abundance ratios (e.g. Pritzl et al. 2005), and reflects the difference in star formation histories between galaxies with significantly different masses. For this reason, we discuss the LMC training set as three groups, which we divide according to ages previously determined using other techniques: old (>5 Gyrs), intermediate age (1-4 Gyrs) and young (< 1 Gyr). Coordinates, photometric properties, and previous abundance information that is available in the literature are given in Table 1.

As for the MW training set, we have only observed the core regions of the LMC clusters (see § 3). Because of this, and because the clusters are lower mass and lower density, incomplete sampling is a potential complication for integrated light analysis that arises from only observing a fraction of the total population of the cluster. Because our analysis method involves using theoretical color magnitude diagrams (CMDs), which accurately represent the full stellar population, incomplete sampling must be explicitly included in our analysis strategy. In this paper, we use the phrase "sampling uncertainties" to refer to statistical fluctuations in the small numbers of bright stars present in the core region of a cluster at the time of our observations. These statistical fluctuations can potentially have a significant impact on the integrated properties of the cluster because the stars are very luminous. In general, the importance of sampling uncertainties scales with the total number of stars in the cluster, and therefore with the total luminosity (M_V^{tot}) of the cluster. In our training set clusters in particular, we have effectively reduced the total luminosity of the clusters by observing only a fraction of the total flux, so we can expect that sampling uncertainties will be a greater issue than they would be for integrated light analysis of distant clusters in which a large well-populated fraction of the cluster will always be observed within one seeing disk.

It is also important to note that sampling uncertainties are more important for clusters of younger ages, due to the contribution of very few, but very luminous giant stars in rapid phases of stellar evolution
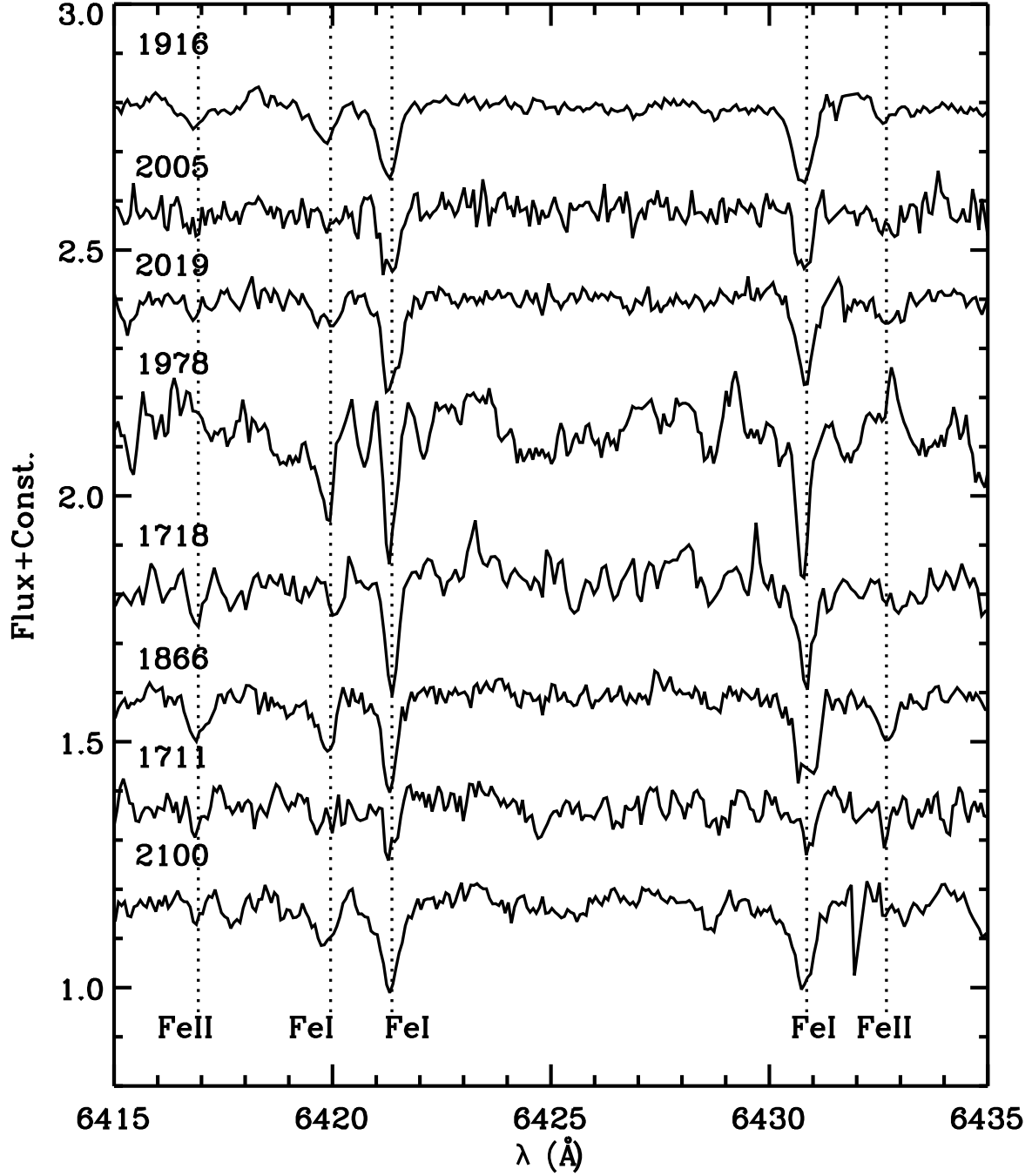
Figure 1. Example LMC cluster spectra shown decreasing in age (top to bottom). Individual Fe I and Fe II lines that can be used in abundance analysis of one or more clusters are marked by dotted lines.

(e.g. see Brocato et al. 1999). Young stellar populations may change significantly over only a <1 Gyr age range (e.g. Brocato et al. 1999; Fagiolini et al. 2007; Bruzual & Charlot 2003). In general, it is necessary to evaluate sampling uncertainties on younger (<5 Gyr) clusters because they will suffer from greater intrinsic statistical fluctuations in the stellar populations than old clusters. For the younger LMC training set clusters in particular, sampling uncertainties will be exacerbated due to observing only a fraction of the total cluster population.

Because statistical fluctuations will always be an issue for young, rapidly evolving clusters, in this work we have extended the integrated light abundance analysis method developed in Paper I and Paper II to include extensive tests designed to address sampling uncertainties in the LMC training set. These tests will be discussed further in § 4. We aim to evaluate how sampling uncertainties in the young LMC training set clusters affect the constraints we can derive for the cluster ages and abundances.

Finally, we note that in this work on the LMC training set, we do not analyze the IL spectra using resolved star photometry as we did for the MW training set in Paper I and Paper II. This is mainly due to the fact that in the core regions we have observed, the quality of the available photometry is not high enough to make this analysis meaningful, with the possible exception of the deep Hubble Space Telescope (HST) photometry for NGC 1978, by Mucciarelli et al. (2007). At the distance of the LMC crowding in the cluster core regions always makes the photometry incomplete for main sequence stars. Moreover, as discussed in Paper II, even tests with the best photometry of Galactic GCs (e.g. Piotto et al. 2002; Sarajedini et al. 2007) result in a higher scatter in our abundance solutions than tests performed with isochrones. Thus, for clusters in the LMC training set, we limit ourselves to broad consistency checks with the available photometry, discussed in detail in § 5.2.

In summary, when compared to the MW training set, first we expect that the old LMC clusters will be more difficult to analyze due to lower S/N data. Second, we expect that the method strategy will be very similar to the MW training set strategy except for the addition of sampling uncertainty tests developed in this work. We will discuss the extent that these tests can improve our abundance solutions by allowing for statistical variations in the stellar populations. For clusters <5 Gyr old, we expect that the analysis will be more challenging than for the old clusters because the stellar populations may change significantly over only a <1 Gyr age range. This age sensitivity means that it is crucial to test the IL method on younger clusters in order to assess how well the ages and abundances can be constrained, and to further develop the IL analysis strategy if needed.

3. OBSERVATIONS AND DATA REDUCTION

All of the data for the LMC training set clusters, with the exception of NGC 1718, were obtained using the echelle spectrograph on the 2.5 m du Pont telescope at Las Campanas during dark time in 2000 December and 2001 January. The wavelength coverage of these spectra is approximately 3700–7800 Å.

As done for the MW training set clusters, the LMC cluster cores were scanned to obtain IL spectra (Paper I).

Table 2
Observation Log and Estimated S/N

Cluster	Exposure (s)	S/N (pixel^{-1})		
		4380 Å	6100 Å	7550 Å
NGC 2019	20,218	30	70	70
NGC 2005	22,010	20	50	60
NGC 1916	22,785	40	80	90
NGC 1978	50,150	20	50	60
NGC 1718	19,560	80	60	80
NGC 1866	41,230	50	80	70
NGC 1711	18,350	40	50	50
NGC 2100	20,800	50	70	70
NGC 2002	18,357	60	110	140

Table 3
Cluster Structural Parameters And Fraction Observed

Cluster	c[1] arcsec	R_{King}[1] arcsec	R_{core}[2] arcsec	Fraction Observed
NGC 2019	1.68	2.56	3.61	0.45
NGC 2005	1.53	2.96	3.63	0.60
NGC 1916	1.47	3.02	3.35	0.62
NGC 1978	⋯	⋯	⋯	0.05-0.10
NGC 1718	1.33	10.32	8.52	0.23
NGC 1866	1.65	11.97	14.15	0.14
NGC 1711	1.44	8.35	8.78	0.16
NGC 2100	1.74	4.23	5.02	0.40

Note. — 1. From McLaughlin & van der Marel (2005). The concentration parameter is defined as c $\equiv \log_{10}(R_{tidal}/R_{King})$., 2. Cluster core radii from Mackey & Gilmore (2003).

Because of the greater distance to the LMC clusters, we scanned a 12×12 arcsec^2 or 8×8 arcsec^2 region of the cluster cores, instead of the 32×32 arcsec^2 region scanned in MW clusters. Our spectra were reduced with standard IRAF[2] routines, combined with the scattered-light subtraction described in Paper I. The observational technique and data reduction are described in further detail in Paper I and Paper II.

NGC 1718 was observed with the MIKE double echelle spectrograph (Bernstein et al. 2003) on the 6.5 m Magellan Clay telescope in 2006 November. The integrated light spectrum was obtained by scanning the central 12×12 arcsec^2 region of NGC 1718 using a modification to the telescope guiding program provided by D. Osip. The blue side wavelength coverage is 3350–5050 Å, and the red side wavelength coverage is 4800–9000 Å. We used a slit size of 1".0 × 5".0, and 3×2 pixel on-chip binning. The data were reduced using the MIKE Redux pipeline (Bernstein et al. 2011, in preparation), an extended library of spectroscopic routines building on the SDSS pipeline and developed for a number of instruments by J. X. Prochaska.[3]

Exposure times for each cluster and approximate S/N values at three regions in each spectrum are listed in Table 2. For all clusters we primarily use the higher S/N

[2] IRAF is distributed by the National Optical Astronomy Observatories, which are operated by the Association of Universities for Research in Astronomy, Inc., under cooperative agreement with the National Science Foundation.
[3] http://www.ucolick.org/∼xavier/IDL/index.html

data > 4400 Å for our abundance analysis. Example spectra for the clusters are shown in Figure 1.

We have calculated the total V-band flux contained in the scanned region for each cluster (with the exception of NGC 1978) using the surface brightness profiles uniformly measured by McLaughlin & van der Marel (2005). The cluster surface brightness profile parameters and core radii (Mackey & Gilmore 2003) are listed with the calculated fraction of flux observed in Table 3. A surface brightness profile was unavailable for NGC 1978. To estimate the flux we observed we compare the HST photometry (kindly provided by A. Mucciarelli) to the other clusters in our MW and LMC training set. While the exact fraction for NGC 1978 is uncertain, it is clearly small and in the range of 5 to 10%. The S/N of our data for NGC 1978 is also lower than for most of the other clusters in the sample due to its smaller total luminosity and surface brightness. The combination of lower data quality and undersampling makes analysis of NGC 1978 particularly challenging, which we discuss further in § 4.5.

4. ABUNDANCE ANALYSIS

The method that we have developed for measuring detailed abundances from the integrated light spectra of GCs is extensively described in Paper I, Paper II and Colucci et al. (2009). We briefly review that strategy In § 4.1-§ 4.3. In § 4.4 we discuss the results for the older clusters of the LMC training set. We also develop an additional technique to address incomplete sampling effects, which we also apply to the intermediate age and younger clusters in § 4.5 and § 4.6.

4.1. *EWs and Line Lists*

As in all of our previous work on IL spectra, we use the semi-automated program GETJOB (McWilliam et al. 1995) to measure absorption line equivalent widths (EWs) for individual lines in the IL spectra. Continuum regions for each spectral order are interactively fit with low order polynomials and line profiles are fit with single, double, or triple Gaussians. We take special care in continuum placement and attention to line blending due to the nature of IL spectra. Line lists were taken from Meléndez & Barbuy (2009), Paper II, Colucci et al. (2009), and references therein. The lines and EWs used in our final analysis for each cluster can be found in Table 4.

4.2. *Constructing CMDs and EW Synthesis*

Our abundance analysis technique allows us to calculate [Fe/H] solutions for any synthetic cluster population, without a priori knowledge of the true cluster population. The synthetic populations are used to synthesize IL EWs, which are compared to our observed IL EWs during our abundance analysis. We construct synthetic populations using the single age, single metallicity theoretical isochrones from the Teramo[4] group (Pietrinferni et al. 2004, 2006; Cordier et al. 2007). The isochrones we employ also contain an extended asymptotic giant branch (AGB), $\alpha-$enhanced low$-$temperature opacities calculated according to Ferguson et al. (2005), and mass$-$loss parameter of η=0.2.

---

[4] Teramo isochrones downloadable at http://albione.oa-teramo.inaf.it/

The Teramo isochrones are tabulated with two treatments of convection at the border of convective stellar cores, which can be important because the choice of treatment can affect the morphology of main sequence turnoffs and blue loop populations of younger clusters (Pietrinferni et al. 2004). The first, most simplistic treatment, is used in the "canonical" tracks. In this case, convective instability is treated using the Schwarzschild criterion, which results in a convective core with a clean boundary that is determined by the input stellar physics. The second treatment, used in the "non-canonical" tracks, parametrizes a certain amount of mechanical convective overshooting past the Schwarzschild boundary. This overshooting can occur if fluid elements maintain some velocity past the Schwarzschild boundary, and/or if there is some rotationally induced mixing beyond the boundary (Meynet & Maeder 2000). Convective overshooting effectively increases the size of the stellar core, resulting in a brighter luminosity and shorter lifetime. Note that the presence or degree of convective overshooting only affects stars with masses larger than $\sim 1.1 M_{\odot}$, because only these stars are hot enough to develop a convective core during the H-burning phase. This means that the treatment of convective overshooting only impacts the CMDs of clusters younger than $\sim$3 Gyr.

In Paper II and Colucci et al. (2009) we analyzed clusters with ages >5 Gyr, and chose to use the Teramo canonical evolutionary tracks. This choice did not significantly affect our analysis because of the older ages and cooler temperatures of the stars in these clusters. While the presence or degree of convective overshooting required to match observations is still under debate (Testa et al. 1999; Barmina et al. 2002), Mucciarelli et al. (2007) found the non-canonical Teramo isochrones to be a better match than the canonical isochrones to the turnoff region of their high precision HST photometry of NGC 1978. Therefore, in this work we have chosen to use the non-canonical isochrones for the younger clusters in order to be consistent with results from the best available photometry. In §5 we briefly discuss uncertainties due to our choice of isochrones.

In our analysis, synthetic CMDs are created by combining the model isochrones with an initial mass function (IMF) of the form in Kroupa (2002). For the MW clusters in Paper I and Paper II, we made an additional correction for mass segregation in the cluster cores due to the small fraction of the stellar populations we observed. For the LMC training set clusters we do not make a mass segregation correction. This correction is not necessary in the older LMC clusters because we have observed a larger fraction of the cluster population, and it is not necessary for the younger clusters because we do not expect mass segregation due to dynamical evolution to be as significant an effect over their shorter lifetimes, as the timescales for central and half-mass relaxation time are several hundred Myr and $\sim$3 Gyr, respectively (e.g. Fischer et al. 1992). For simplicity and self-consistency, in this analysis we ignore the possibility of primordial mass segregation (Vesperini et al. 2009).

Synthetic CMDs are created for the available range of age and metallicity of the Teramo isochrones. Each CMD is divided into $\sim$25 equal flux boxes containing stars of similar properties. The properties of a flux-weighted "average" star for each box are used in the

Table 4
Line Parameters and Integrated Light Equivalent Widths for LMC GCs

Species	λ (Å)	E.P. (eV)	log gf	EW (mÅ) 1916	EW (mÅ) 2005	EW (mÅ) 2019	EW (mÅ) 1978	EW (mÅ) 1718	EW (mÅ) 1866	EW (mÅ) 1711	EW (mÅ) 2100	EW (mÅ) 2002
Fe I	6265.141	2.180	-2.532	⋯	⋯	⋯	⋯	86.3	⋯	⋯	87.5	⋯
Fe I	6311.504	2.830	-3.153	⋯	⋯	⋯	⋯	⋯	54.7	⋯	⋯	⋯
Fe I	6322.694	2.590	-2.438	⋯	36.3	47.7	128.7	⋯	58.9	47.4	63.4	⋯
Fe I	6330.852	4.730	-1.640	⋯	⋯	⋯	⋯	⋯	23.7	⋯	⋯	33.0
Fe I	6335.337	2.200	-2.175	74.2	58.6	67.4	135.6	74.1	67.3	53.5	⋯	⋯
Fe I	6336.830	3.690	-0.667	59.5	⋯	⋯	134.6	65.8	68.7	40.4	⋯	⋯
Fe I	6353.849	0.910	-6.360	⋯	⋯	⋯	⋯	⋯	86.5	⋯	⋯	⋯
Fe I	6355.035	2.840	-2.328	60.7	⋯	49.6	⋯	68.0	46.5	⋯	93.1	⋯
Fe I	6380.750	4.190	-1.366	⋯	⋯	⋯	⋯	⋯	42.7	⋯	⋯	⋯
Fe I	6392.538	2.280	-3.957	⋯	⋯	⋯	⋯	30.2	⋯	⋯	⋯	⋯

Note. — Table 4 is presented in its entirety at the end of the text. Lines listed twice correspond to those measured in adjacent orders with overlapping wavelength coverage.

IL EW synthesis, which we perform with ILABUNDS (Paper I). ILABUNDs employs the 2010 version of the spectral synthesis code MOOG (Sneden 1973). We use the ODFNEW and AODFNEW model stellar atmospheres of Kurucz [5] (e.g. Castelli & Kurucz 2004) for all abundance analysis.

To begin the analysis of any cluster, we calculate a mean [Fe/H] abundance from all available Fe I lines for the large grid of synthetic CMDs. We note that because we measure far fewer Fe II lines than Fe I lines, we do not use Fe II lines to constrain the best-fitting CMD. The abundances we measure from Fe II lines are therefore presented in Paper IV. We next use the quality of the Fe I abundance solution to constrain the best-fitting age and abundance for each cluster. As in our previous work, all abundances are calculated under the assumption of local thermodynamic equilibrium (LTE). We only include Fe I lines with EWs<150 mÅ (see Paper II) in order to avoid line saturation problems.

4.3. *Determining the Best-Fitting CMD*

The first step in this procedure is to determine one synthetic CMD for each age that has the best-fitting metallicity. Our analysis of the MW training set (Paper II) has shown that the best strategy for consistently identifying the best-fitting CMD for each age is to require that the abundance used in constructing the isochrones be consistent with the abundance recovered by our analysis (see also Colucci et al. 2009). This is essentially taking advantage of the fact that the dependence of the RGB on metallicity is relatively well understood (e.g. Gallart et al. 2005), and that RGB stars have an important influence on Fe I line strengths in IL spectra. Hereafter, we refer to the solutions where [Fe/H]$_{iso}$=[Fe/H]$_{cluster}$ as "self-consistent" Fe abundance solutions. Often, it is clear that the self-consistent solution lies at a metallicity in between two synthetic CMDs in our grid. When this occurs, we calculate an isochrone with the appropriate metallicity according to the interpolation scheme recommended by Pietrinferni et al. (2006).

After constraining the best-fitting synthetic CMD properties from an initial grid of ∼70 possibilities to a single [Fe/H] for each age, we are able to isolate the most appropriate age(s) out of these 8 solutions using Fe line diagnostics. These diagnostics, which are commonly used in standard stellar abundance analyses, relate to the quality of the [Fe/H] solutions. In particular, a stable [Fe/H] solution should not depend on the parameters of individual lines (excitation potentials, wavelengths, or reduced EWs[6]), and the standard deviation of the [Fe/H] solution should be small. Correlations of [Fe/H] with excitation potential (EP), wavelength, and reduced EW are indicative of improper distributions of stellar temperatures or gravities in the synthetic CMDs as compared to the actual clusters. In general, these effects are difficult if not impossible to disentangle without additional constraints, although we will discuss them in the context of incomplete sampling in § 4.4.1. For the purposes of constraining the best-fitting CMD, we consider synthetic CMDs that minimize these correlations to be most representative of the cluster stellar population. To that end, for each synthetic CMD solution, we perform a linear least-squares fit to [Fe/H] versus EP, wavelength, reduced EW. We then use the magnitude of the slope in these fits for our Fe line diagnostics, along with the standard deviation of the mean [Fe/H] of the Fe I lines. We find that these 4 diagnostics are usually strongly correlated with each other, which provides a means to identify the most appropriate synthetic CMD using Fe lines alone.

4.4. *Results: Old Clusters*

For old clusters (>10 Gyrs), the analysis method developed in Papers I and II and described above can unambiguously identify an accurate CMD for the analysis of the integrated light spectra. Several of the clusters in the LMC sample discussed here are in that age range. The LMC sample presents some challenges to this basic analysis in that even old clusters in this sample are in some cases sparsely sampled due to low surface brightness or low total mass. For that reason, our analysis results can be improved even for these old clusters by allowing for a statistically incomplete sampling of the CMD. We present an additional strategy for allowing for incomplete sampling, and address the issues for each cluster below.

---

[5] The models are available from R. L. Kurucz's Website at http://kurucz.harvard.edu/grids.html

[6] Reduced EW ≡ log(EW / λ)
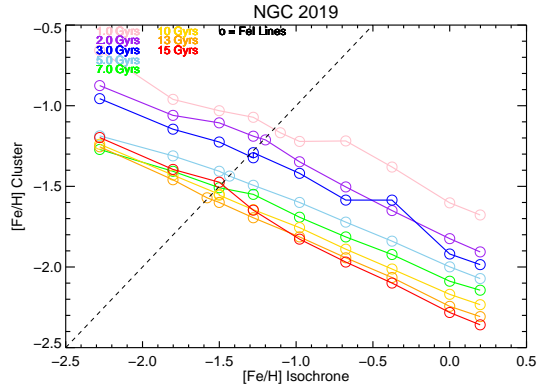
Figure 2. Abundance solutions for Fe I lines for NGC 2019. Colors correspond to CMDs of different ages, as labeled. Self-consistent solutions are found where the output [Fe/H]$_{\text{cluster}}$ solution equals the input [Fe/H]$_{\text{iso}}$ abundance of the isochrone. These solutions fall on the dashed black 1:1 line.

4.4.1. NGC 2019

NGC 2019 is an old, moderately metal-poor cluster with a total luminosity of $M_V^{\text{tot}} \sim -8$ (Olsen et al. 1998; Pessev et al. 2008). However, it is also a good test case for demonstrating the need for accounting for sampling uncertainties in an integrated light analysis. We calculate that we have observed $\sim 45\%$ of the total flux of NGC 2019, which means that this cluster has the most sampling incompleteness of the old clusters in the LMC training set because it has the fewest number of stars in each synthetic CMD.

We begin our analysis by determining the best-fitting CMD following our standard method. In Figure 2, we show the [Fe/H] solutions for the grid of synthetic CMDs described in § 4.2, which span a range in age of 1-15 Gyr, and range in metallicity of $-2.6 \leq$[Fe/H]$\leq +0.2$. The CMDs with self-consistent [Fe/H] solutions (i.e. [Fe/H]$_{\text{iso}}$=[Fe/H]$_{\text{cluster}}$), lie on the dashed line in Figure 2. By requiring self-consistency in the [Fe/H] solution, we have narrowed down the grid of synthetic CMDs to one acceptable CMD for each age. To determine which of the 8 self-consistent CMDs is the best match to the stellar population of NGC 2019, we next compare the Fe line diagnostics. These diagnostics are shown in Figure 3. Each diagnostic has been normalized to its worst value in order to show all 4 diagnostics on the same scale. The diagnostics in Figure 3 show similarities to the diagnostics found for other old clusters in the MW training set in Paper II and for old clusters in M31 (Colucci et al. 2009). The best diagnostics for NGC 2019 are found for ages $\geq$5 Gyr. While 5 to 15 Gyr is a much broader range in age than we found for MW clusters, it can be seen in Figure 2 that the difference in [Fe/H] between the 5 and 15 Gyr synthetic CMDs is only $\sim$0.15 dex, which means that the metallicity of NGC 2019 is already very well constrained.

We note that, as in our previous work, we find that the best solutions are for ages >5 Gyr, even though the behavior of the diagnostics fluctuates somewhat, or in some cases the diagnostics don't completely agree with each other. This is expected, as there are some properties of the theoretical stellar populations that don't exactly match the true stellar populations in the cluster, and the different diagnostics are sensitive to different stellar
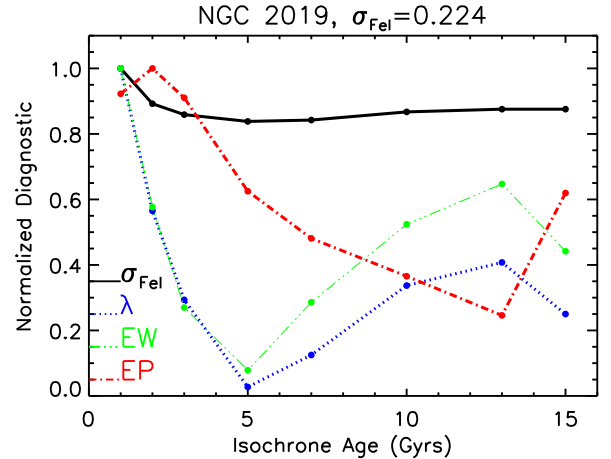
Figure 3. Fe abundance diagnostics for self-consistent solutions for NGC 2019. Each diagnostic has been normalized to its maximum, or worst, value in order to show all diagnostics on the same scale. Solid black line shows σ_{Fe}, dotted blue line is the slope in [Fe/H] vs. λ, red dash-dot line is the slope in [Fe/H] vs. EP, and the green dash-triple dot line is the slope in [Fe/H] vs. reduced EW (log(EW/wavelength)). The best solutions are found for ages > 5 Gyr.

types. More uncertain aspects of the isochrones can include AGB stars, which we discuss below for NGC 2019, or blue horizontal branch stars and blue stragglers, which we discuss in more detail for NGC 2005 in §4.4.2.

We next investigate the effect of incomplete sampling on the age and abundance solutions for NGC 2019. We note that for old, low luminosity clusters, the most important sampling uncertainties will be fluctuations in the number and type of evolved stars, particularly luminous AGB stars and RGB stars (Brocato et al. 2000). Here we will explore tests to improve our solution by accounting for statistical fluctuations in luminous evolved stars. Although these tests are probably unnecessary for the analysis of more distant, and thus better sampled, extragalactic clusters, they can be applied with no a priori knowledge of the CMD, and therefore can be easily generalized for the analysis of any cluster.

In order to allow the synthetic CMD stellar populations to vary in a meaningful way, we use a Monte Carlo technique to statistically populate the cluster IMF with discrete numbers of stars. The total number of stars in each synthetic CMD is normalized so that the total flux in the CMD is consistent with the observed M_V^{tot} of the cluster, modulated by the observed flux fraction. When reducing the total flux of the cluster to be consistent with the observed region, we have assumed that stars of different masses are evenly distributed throughout the cluster. An important difference between generating the synthetic CMDs using a Monte Carlo method versus the technique used for the original analysis method developed in Paper I and Paper II, is that the Monte Carlo method creates CMD boxes with integer numbers of stars. The original method creates average CMD boxes with non-integer numbers of stars, with the constraint that the number of stars in each box must be ≥ 1.0. To illustrate this point, in Table 5 we compare the synthetic CMD created using the original method for a 10 Gyr, [Fe/H]=-1.5 isochrone, to a synthetic CMD created using the Monte Carlo technique. As expected, the significant differences

Table 5
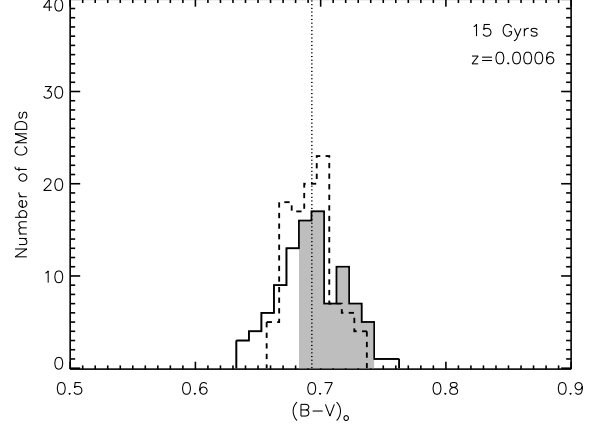Synthetic CMD Comparison

Box	Averaged			Monte Carlo		
	M_V	$B-V$	N_{stars}	M_V	$B-V$	N_{stars}
1	7.178	0.865	19033.70	7.188	0.868	18867
2	6.211	0.640	7343.58	6.215	0.641	7439
3	5.640	0.520	4460.14	5.651	0.521	4325
4	5.208	0.455	2913.89	5.231	0.458	3025
5	4.836	0.414	2185.18	4.863	0.417	2169
6	4.488	0.384	1596.35	4.520	0.386	1596
7	4.165	0.360	1234.24	4.200	0.363	1212
8	3.875	0.346	853.19	3.901	0.347	867
9	3.592	0.349	661.95	3.616	0.348	665
10	3.290	0.404	492.02	3.333	0.389	508
11	2.876	0.593	340.62	2.977	0.567	370
12	2.056	0.674	160.46	2.231	0.665	187
13	1.310	0.719	81.82	1.478	0.708	99
14	0.653	0.771	44.14	0.888	0.750	55
15	0.101	0.830	26.12	0.319	0.805	33
16	−0.235	0.871	19.25	−0.104	0.854	22
17	−0.743	0.948	12.11	−0.453	0.902	16
18	−1.204	1.033	7.90	−0.897	0.975	11
19	−1.623	1.124	5.35	−1.289	1.051	8
20	−2.009	1.225	3.82	−1.815	1.173	5
21	−2.344	1.339	2.80	−2.455	1.387	3
22	−2.606	1.448	1.88	0.442	0.569	36
23	0.185	0.629	31.98	0.430	0.532	35
24	0.430	0.530	35.19	0.400	0.531	34
25	0.404	0.528	34.44	−0.231	0.732	23
26	0.071	0.653	26.34	−1.552	1.048	6
27	−1.258	0.981	7.93	−2.676	1.514	3
28	−2.583	1.520	2.28	⋯	⋯	⋯

Figure 4. Histogram of integrated $(B-V)_0$ color for 100 CMD realizations of a 15 Gyr, z=0.0006, ([Fe/H]=−1.5) isochrone. Solid black line shows the histogram for a population where the total flux in stars has been normalized to 45% of a $M_V^{\mathrm{tot}}=-8$ cluster, which is appropriate for our integrated light spectrum of NGC 2019. Dashed black line shows the histogram for a population normalized to 100% of a $M_V^{\mathrm{tot}}=-8$ cluster. CMDs with $(B-V)_0$ color consistent with the observed, reddening-corrected $B-V$ of NGC 2019 are shaded in gray. The $(B-V)_0$ of the average CMD is marked by the dotted line, and is consistent with the peak in both histograms for the CMD realizations, as it represents an average population.

between the two CMDs occur for the luminous ($M_V \leq 0$) boxes representing the upper RGB and AGB stars. Most of these boxes were created by averaging the properties of 10 stars or less, and thus are particularly sensitive to small number statistics. In the example comparison in Table 5, the CMD created using the Monte-Carlo technique has one less box than the CMD created using the original technique, due to the redistribution of the luminous stars in boxes 17 through 28.

To approximately assess the impact of sampling uncertainties, we have decided to create 100 synthetic CMDs for each isochrone of interest using the Monte-Carlo technique. We will refer to these CMDs created using the Monte-Carlo technique as "CMD realizations." For clarity, we will refer to synthetic CMDs created using the original technique as "average CMDs."

One way to evaluate the effect of under-sampling the population is to compare the level of statistical fluctuations in the intrinsic, integrated color, which is defined here as "$(B-V)_0$." For example, Brocato et al. (1999, 2000) evaluated the statistical fluctuations in the integrated colors of cluster CMDs that were created using a Monte Carlo technique similar to the procedure used here. They found that the integrated colors showed large variations for CMDs created with less than 30,000 stars. We show the variation in $(B-V)_0$ for 100 CMD realizations of one of the best-fitting CMDs for NGC 2019 in Figure 4. The CMD realizations, shown by the solid line, were created using the best-fitting CMD with an age of 15 Gyr, and [Fe/H]=−1.5, and show a spread in $(B-V)_0$ of ∼0.13 mag. Note that the number of stars in each of the CMDs included in the solid line histogram were normalized to correspond to 45% of the flux of a $M_V^{\mathrm{tot}} \sim -8$ cluster, which corresponds to the observed flux of NGC

2019. To evaluate the spread in $(B-V)_0$ that results from our incomplete sampling, we also create CMD realizations normalized to 100% of a $M_V^{\mathrm{tot}} \sim -8$ cluster. These more luminous CMD realizations are shown by the dashed line histogram in Figure 4. The spread in $(B-V)_0$ of these more luminous CMD realizations is ∼0.08 mag, which, as expected, is a smaller range. As a sanity check, we also mark the $(B-V)_0$ of the average CMD created using the original technique with a dotted line in Figure 4. We note that the $(B-V)_0 = 0.69$ of the average CMD is consistent with the $(B-V)_0$ of the peak in both CMD realization histograms, which we would expect because this CMD represents an average population for the isochrone.

After creating CMD realizations for a given isochrone, an appropriate subset of CMD solutions can be identified by applying other observable constraints. As a first constraint, we impose the self-consistency requirement used in our original method. This constraint must be reapplied to the [Fe/H] abundance solutions for the CMD realizations because the redistribution of luminous, cool giants in the CMD realizations results in a spread in the derived output [Fe/H]. The results for the CMD realizations of NGC 2019 are shown in Figure 5, with the average CMD solutions from Figure 2 for reference. We have marked the CMD realizations that meet the self-consistency requirement as black circles in Figure 5.

The spread in derived [Fe/H] is not unexpected, because cool giants have a strong influence on the flux-weighted Fe I EWs, which was discussed in Paper I. To clarify this point in the context of sampling uncertainties, in Figure 6 we show the EW fraction contributed from different regions of the CMD for different Fe lines. The lines have been chosen to illustrate the importance of different types of stars on different lines. Four lines are plotted, which have very different combinations of wave-
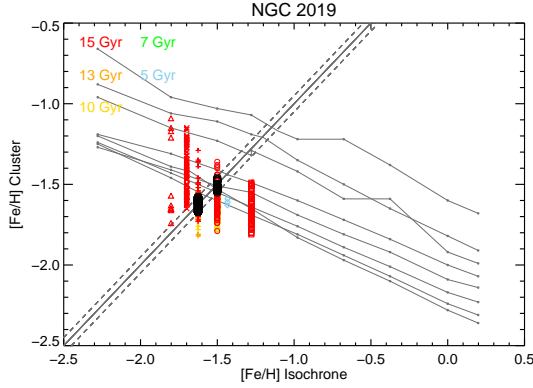
Figure 5. Same as Figure 2, with the addition of the Fe I abundance results for the CMD realizations of NGC 2019. Red points correspond to 15 Gyr CMD realizations. Only CMD realizations consistent with the observed $B - V$ color of NGC 2019 are shown. Black circles on the solid black 1:1 line denote CMD realizations that satisfy the self-consistent criterion $[Fe/H]_{iso}=[Fe/H]_{cluster}$, and are therefore possible solutions for the population of NGC 2019.

length and EP. This emphasizes how redistributions of luminous, cool giants can affect the [Fe/H] vs. EP and [Fe/H] vs. wavelength diagnostics. In general, Figure 6 demonstrates that the RGB and AGB CMD boxes dominate ($\sim 80\%$) the Fe I EWs. More subtle is the fact that high EP and bluer wavelength Fe I lines are slightly less sensitive to AGB and RGB boxes than low EP and redder wavelength lines. The high EP and bluer wavelength lines are more sensitive to the main sequence (MS) and horizontal branch (HB) boxes than the low EP and redder wavelength lines, because they have stars at hotter temperatures. The sensitivity of the Fe I line abundances to small redistributions of flux between the AGB, RGB and HB means that different CMD realizations result in a spread in mean [Fe/H], but also that the Fe line diagnostics are in principle sensitive to whether a statistically rare CMD realization results in an improvement in the overall stability of the [Fe/H] solution.

From this exercise it is apparent that there may be self-consistent CMD realizations that exist at different [Fe/H] than our original solution. It is therefore necessary to follow the procedure outlined above for a range of isochrone metallicity (and ages if warranted). In the case of NGC 2019, we have done this for isochrones with [Fe/H]$=-1.8$ to -1.3 and for ages between 5 to 15 Gyr, which can be seen in Figure 5.

After we have eliminated CMD realizations based on our [Fe/H] self-consistency requirement, we can eliminate additional CMDs based on their consistency with the cluster's observed, reddening-corrected integrated color. CMD realizations for NGC 2019 that are consistent with the observed $B - V$ from the catalog of Pessev et al. (2008), and the $E(B - V)$ determined by Olsen et al. (1998) are shaded in gray in the histogram in Figure 4. In this case, we note that the $(B - V)_0$ of the average CMD is also consistent with the observed $B - V$ of NGC 2019, which is a hint that the average CMD may already be a reasonable match. The original average CMD solutions at ages of 5 and 7 Gyr have integrated $(B-V)_0$ colors that are inconsistent with the observed $B - V$. This is apparent in Figure 7, in which the average 5 and 7 Gyr solutions, which are marked as filled black circles,

are outside the shaded gray region corresponding to the observed $B - V$. While there are some CMD realizations with an age of 7 Gyr that do satisfy the $(B - V)_0$ requirement, in general there are many fewer acceptable 7 Gyr CMD realizations than there are for ages >10 Gyr. In other words, while NGC 2019 may have an age of 5 Gyr, this possibility is statistically unlikely according to our analysis.

We find 120 CMD realizations for isochrones with ages of $7-15$ Gyr and $[Fe/H]_{iso} = -1.6$ to -1.5 that are consistent with the observed $(B - V)_0$ of NGC 2019 and also result in a self-consistent [Fe/H] solution. We next identify the best-fitting CMD(s) for each age using the Fe diagnostics introduced in § 4.3. In Figure 8 we show the normalized Fe I diagnostics for the 120 CMD realizations, which we have designated CMDs 0 through 119. As was the case for the original 8 average CMD solutions, the most stable CMD realizations are those that minimize all of the diagnostics simultaneously. We highlight the best-fitting, most stable solution for each age with dashed lines in Figure 8. In the case of NGC 2019 we find that for ages of 7, 10 and 15 Gyrs the best-fitting CMD realization has an input $[Fe/H]_{iso} = -1.6$, which is 0.1 dex lower than the $[Fe/H]_{iso}$ of the best-fitting average CMD solutions. For an age of 13 Gyrs the best-fitting solution has an input $[Fe/H]_{iso} = -1.5$, which is the same as for the original average CMD solution. The statistical line-to-line scatter in Fe abundance, or σ_{Fe}, is 0.20 dex.

After constraining the 120 self-consistent CMD realizations to a single best-fitting CMD realization for each age between 7 to 15 Gyr, we can compare the normalized diagnostics in order to identify the best-fitting age(s) for NGC 2019, similar to what we did for the average CMD solutions at the beginning of this section. Figure 9 shows the diagnostics for the original 1 to 5 Gyr solutions compared to the diagnostics for the best-fitting CMD realizations at ages of 7 to 15 Gyr. The main differences between Figure 3 and Figure 9 are that the diagnostics for ages of 7 to 15 Gyrs are clearly much more strongly correlated with each other, and that the CMDs with ages of 7, 10 and 15 Gyrs result in more stable [Fe/H] solutions than the original average CMD solutions. Our final solution is constrained to two possible synthetic CMDs with ages of 7 to 10 Gyrs.

For reference, in Figure 10 we show the [Fe/H] solutions as a function of EP, wavelength and reduced EW for the original average 15 Gyr solution, as well as the best-fitting 10 Gyr CMD realization. It is visually apparent in Figure 10 that for the 10 Gyr CMD realization the σ_{Fe} is reduced and the dependence of [Fe/H] on EP, wavelength and reduced EW is significantly smaller. Therefore, we choose to use the 10 Gyr CMD realization as our final best-fitting CMD, which will be used for calculating the abundances of all other elements in Paper IV.

We are able to find a much more stable solution for NGC 2019 when allowing for sampling uncertainties because of the different contributions of RGB and AGB stars to the flux in different Fe lines. In principle, we can not only identify the most stable solution, but also evaluate whether statistically rare, but cool AGB stars may be present in a cluster. To understand why, it is helpful to revisit the solutions for NGC 2019 in Figure 6. The right panels of Figure 6 show the synthetic CMDs for the original 15 and 10 Gyr solutions, as well as a 15
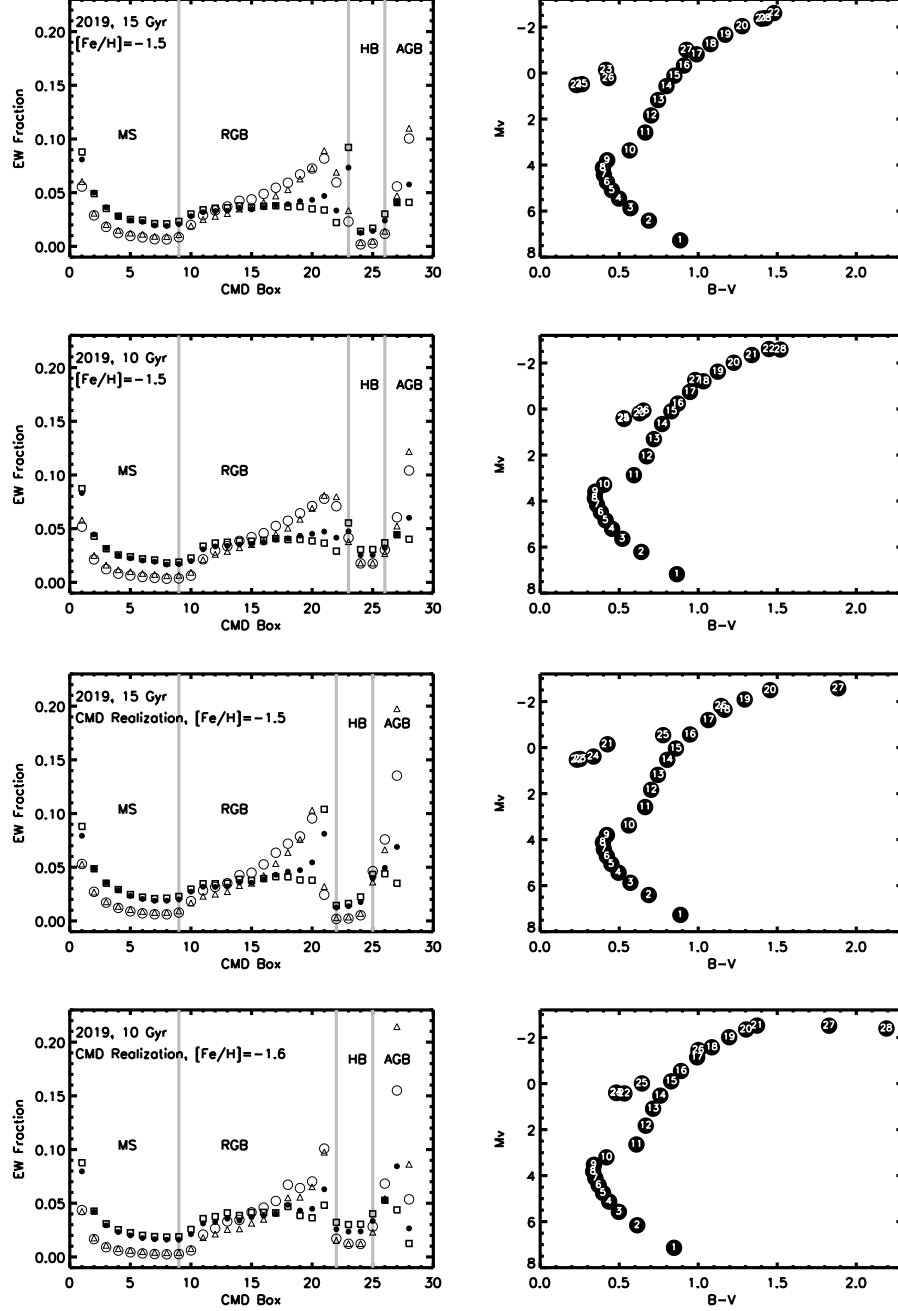
Figure 6. Fe I EW strength for synthetic CMD boxes. Left panels show the contribution of each synthetic CMD box to the total EW fraction of an Fe I line, and right panels show the associated synthetic CMDs, with the box numbers labeled. In the left panels, for an EP comparison, the 5307 Å Fe I line (EP=1.60 eV), and 5383 Å Fe I line (EP=4.3eV), are shown by open and filled circles respectively. For a wavelength comparison, the 4494 Å Fe I line (EP=2.20 eV), and 6677 Å Fe I line (EP=2.70) are shown by open squares and open triangles, respectively. The RGB and AGB CMD boxes dominate the contribution to the Fe I line EWs. Top two rows correspond to the average CMDs with ages of 15 and 10 Gyr, respectively, and [Fe/H]=−1.5. Third row corresponds to the best-fitting CMD realization for NGC 2019 with an age of 15 Gyr and [Fe/H]=−1.5, and the bottom row corresponds to the best-fitting CMD realization with an age of 10 Gyr and [FeH]=−1.6.
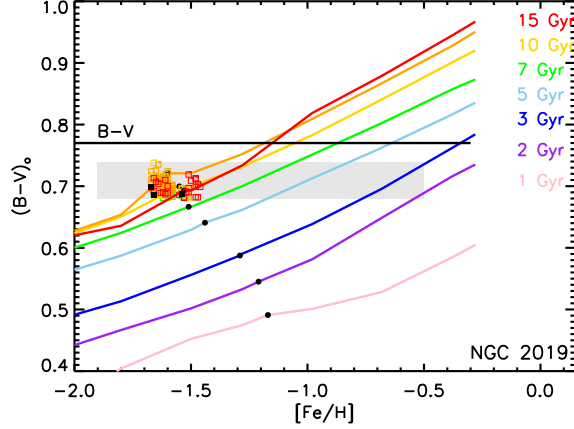
Figure 7. Integrated $(B-V)_0$ colors calculated from the grid of synthetic CMDs for NGC 2019, shown as a function of $[Fe/H]_{iso}$ for each age. Colors denote CMDs with the same ages as in Figure 2. Black circles show the $[Fe/H]_{cluster}$ and age solutions determined for the average CMD analysis. Solid horizontal line corresponds to the observed $B-V$ of NGC 2019 from Table 1. Gray shaded region corresponds to the region in $(B-V)_0$ that is consistent with the reddening corrected $B-V$, with photometric uncertainties. Colored square points correspond to the $(B-V)_0$ and $[Fe/H]_{cluster}$ of self-consistent CMD realizations for NGC 2019, while black solid squares correspond to the best-fitting CMD realization for each age.

Gyr CMD realization at the same [Fe/H] of the original solutions, and the best-fitting 10 Gyr CMD realization with a lower [Fe/H]. The original 10 and 15 Gyr solutions are very similar except for the position of the HB boxes, and therefore there are only subtle differences in the Fe I EW fractions in the left panels. However, for both the 15 Gyr and 10 Gyr CMD realizations there are very red, very luminous, and very cool average star boxes on the AGB that are not present in either of the original CMDs. AGB stars at these types of luminosities and temperatures are relatively rare, so for less massive clusters, boxes at these positions in the CMD do not appear for the average CMDs that we construct using our original technique. It is evident from Figure 6 that not only do the AGB stars in the very luminous and very cool boxes contribute significantly to the Fe I EWs, but they contribute especially to the low EP and redder wavelength Fe I line EWs. In the case of NGC 2019, for the original average CMD solutions we found higher [Fe/H] at redder wavelengths, as well as higher [Fe/H] at lower EP. The addition of significant line strength in very red and very cool stars in the synthesized EWs means that lower Fe abundances are required to match the observed EWs for the redder wavelength and lower EP lines. Therefore the result of adding significant cool AGB flux is a decrease in the dependence of [Fe/H] on EP and wavelength. We emphasize that although the predictions of the properties of very cool AGB stars (or M stars) in the isochrones are still uncertain to some degree, our final result does not depend on determining the temperatures and luminosities of these stars precisely. Instead we have isolated a subset of solutions that have $4-10\%$ of the flux averaged at approximately the same temperature and luminosity.

In conclusion, we have calculated age and abundance solutions for synthetic CMDs with a range of age and [Fe/H] for NGC 2019, and found that a stellar population that is 5 to 15 Gyr in age, and has [Fe/H]$= -1.5$ provides
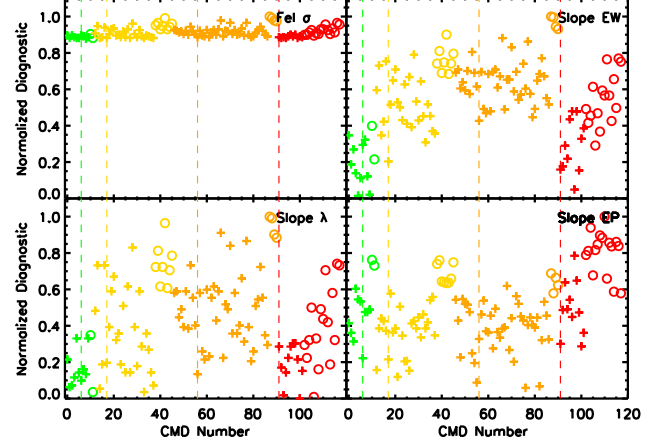
Figure 8. Normalized diagnostics for NGC 2019 CMD realizations that satisfy color and Fe I self-consistency criteria. Symbols and colors are the same as in Figure 5. CMDs are arranged by increasing age, and then by increasing $[Fe/H]_{iso}$ for each age. The best solution for each age is shown by a dashed line, and corresponds to the solution that best minimizes all four diagnostics at once. For NGC 2019, the best solution overall is for an age of 10 Gyr, and [Fe/H]$= -1.6$.

the most self-consistent solution using our original technique. In this section we have described a supplementary technique to evaluate the level of sampling incompleteness for our observations, and performed tests to assess whether the [Fe/H] solutions can be improved by allowing for statistical fluctuations in the stellar population. In the case of NGC 2019, we find that these tests allow us to improve our constraint on the age to 7 to 10 Gyr, as well as determine that a CMD realization with [Fe/H]$=-1.6$ that includes rare and cool AGB stars is a more appropriate match to the stellar population. As shown in Figure 10, the line-to-line scatter is $\sigma_{Fe} = 0.20$ dex. For solutions between 7 and 10 Gyr, we find a maximum difference in [Fe/H] of 0.08 dex, and therefore we quote an uncertainty due to the age of the cluster, σ_{age}, of ± 0.04 dex. In §5 we discuss the final error analysis for all clusters, including statistical uncertainties and systematic errors.

4.4.2. *NGC 2005*

The next LMC training set cluster we analyze is NGC 2005. This and the remaining clusters are all analyzed as outlined for NGC 2019, above. Here we only summarize the final result for the best-fitting CMD solutions.

The diagnostics for the 8, self-consistent, average CMD solutions for NGC 2005 are shown in Figure 11. Like NGC 2019, the diagnostics for the 1 to 3 Gyr CMDs for NGC 2005 show that these are poor solutions. However, there is very little difference in the quality of the solutions between 5 and 15 Gyr, because the RGB morphology is very similar in this age range. The 10 to 15 Gyr average CMD solutions result in [Fe/H]~ -1.6, and the individual diagnostics for the 15 Gyr average CMD solution show a small dependence of [Fe/H] with wavelength, as well as a more significant dependence of [Fe/H] with EP and reduced EW.

The line-to-line scatter of the best abundance solutions is $\sigma_{Fe} \sim 0.25$ dex, which is higher than what we typically obtained for clusters in the MW training set. As dis-
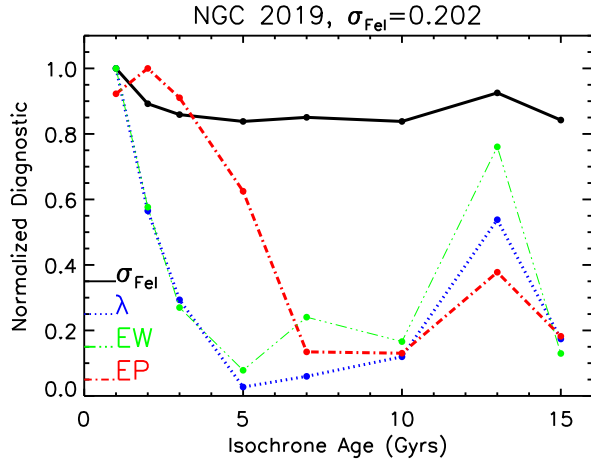
Figure 9. Same as Figure 3, except the solutions shown for ages of 7 to 15 Gyr correspond to the solutions for the best-fitting CMD realizations. The diagnostics for these ages are more correlated with each other than for the average CMD solutions, and the best solutions are found for 7−15 Gyrs.

cussed in § 2, this is probably a consequence of the lower S/N of the LMC training set, and makes NGC 2005 an interesting test case for analysis of clusters with low S/N data. In addition, NGC 2005 is an interesting test case for our new technique to address sampling uncertainties because it has a very blue horizontal branch (HB). In our previous work, we have found that the presence of blue HB stars in a cluster does not significantly affect the [Fe/H] solution because blue HB stars are so hot that they contribute a very small fraction to the IL Fe I EWs. However, in Colucci et al. (2009), we discussed how blue HB stars *can* have a significant effect on the $B - V$ of a cluster, which can be important here because we take the $B - V$ into consideration during our tests for sampling uncertainties. We note that, along with very blue HB stars, blue stragglers are not included in the isochrones used in our analysis. While blue stragglers can also affect the integrated $B - V$ to some degree, it must be kept in mind that they are much less luminous ($\sim$2 magnitudes in V) than blue HB stars, even though they also have very high temperatures. They are also less numerous than blue HB stars (Piotto et al. 2004). We estimate that blue HB stars can account for at most 5-15 % of the total flux, and blue stragglers can only account for at most 2 % of the flux. This means that blue stragglers do not have as significant an effect on the integrated color as blue HB stars. It also means that any conclusions we reach regarding blue HB stars can be extended to blue stragglers as well, to a lesser degree. Finally, it is important to keep in mind that the hot temperatures of blue stragglers also mean that they contribute very little to the Fe I EWs. Thus our analysis is not very sensitive to omitting blue stragglers, in contrast to low resolution line index strategies that utilize Balmer line indexes. In the rest of this section we discuss how the blue HB in particular can affect our sampling uncertainty analysis and keep in mind that our conclusions are generalizable to less luminous blue straggler stars as well.

NGC 2005 is less luminous than NGC 2019 by $\sim$0.5 V mag, and we calculate that we have observed 60% of the total flux. Although NGC 2005 is better sampled than NGC 2019, the 15 Gyr synthetic CMDs have a compa-

rable number of stars ($\sim$40,000) to those of NGC 2019 because it is less luminous overall. Thus, it is possible that incomplete sampling could be affecting our analysis.

First we calculate abundances for CMD realizations created from isochrones with [Fe/H]$= -2.1$ to -1.5 and ages of 5 to 15 Gyr. The range in [Fe/H] of the CMD realizations is small, and the self-consistent solutions have [Fe/H]~ -1.6. We next isolate a subset of CMD realizations with a $(B - V)_0$ consistent with the observed values of $B - V = 0.73$ and $E(B - V) = 0.1$ of Pessev et al. (2008), and Olsen et al. (1998), respectively. The resulting $(B - V)_0$ range allowed for the CMD realizations is shown by the shaded gray area in Figure 12. Inspection of Figure 12 and Figure 7 reveals that although we derive comparable [Fe/H] for both NGC 2005 and NGC 2019, the reddening corrected $B - V$ for NGC 2005 is bluer than that of NGC 2019, which means that the 10 to 15 Gyr average CMD solutions are inconsistent with the observed, reddening corrected $B - V$. There are three possible explanations for this color mismatch: the $E(B - V)$ is not accurate, NGC 2005 has an age of 5 to 7 Gyr, or blue HB stars are affecting the observed color. As mentioned above, we know from the HST CMD of Olsen et al. (1998) that NGC 2005 has a blue HB and that blue HB stars could change the $(B - V)_0$ of the synthetic CMDs by $\sim$ 0.1 dex (Colucci et al. 2009), so this seems like it may be the right explanation. To confirm this hypothesis, we can compare the diagnostics for the self-consistent solutions over the entire age and color range. We find that the best solutions with ages of 5 and 7 Gyr offer only a marginal improvement in the diagnostics over the average CMD solutions at these ages, which implies that a younger age for NGC 2005 is not preferred. For the older ages, we find that the best-fitting CMD realizations have the same $(B - V)_0 \sim 0.67$ as the average CMD solutions, and result in only small improvements in the diagnostics. This confirms that the solution for NGC 2005 was well determined using our original technique, despite the presence of blue HB stars, and that the age range and $(B - V)_0$ are a good match. Moreover, by allowing the $(B - V)_0$ of the CMD realizations to include redder colors, we have also demonstrated that significant flux in cool AGB stars is not needed to improve the solution for NGC 2005.

In conclusion, the final best-fitting CMD we determine for NGC 2005 has an age of 15 Gyr, and [Fe/H]$= -1.6$, although in general we find that we can only constrain the age of NGC 2005 to a 5 to 15 Gyr range. We show the individual Fe line diagnostics for the best-fitting 15 Gyr CMD realization in the bottom panels of Figure 13, so that they can be visually compared to the 15 Gyr average CMD solutions in the top panels. When compared to the average CMD solution, we find that the best-fitting CMD realization has a slightly reduced σ_{Fe}, and the dependence of [Fe/H] on wavelength has disappeared. The dependence of [Fe/H] on EP and reduced EW has decreased, but still remains. It is impossible to tell whether the remaining dependency of [Fe/H] on EP and reduced EW is due to incorrectly modeling the HB, blue stragglers, a more insidious sampling incompleteness, interloping stars, or simply a result of the lower S/N of the data.

It is apparent from the analysis of NGC 2005 that it is important to be aware of the impact of blue HB stars on
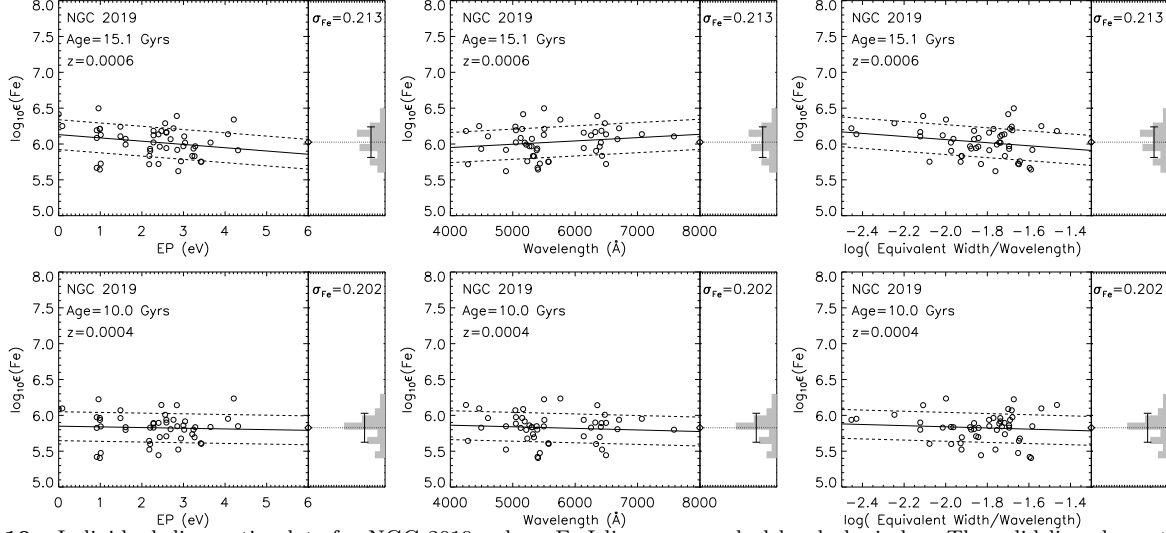
Figure 10. Individual diagnostic plots for NGC 2019, where Fe I lines are marked by dark circles. The solid line shows the linear fit to the Fe I lines and dashed lines show the 1 σ deviation of points around the fit. Diamonds mark the average Fe I abundance. The original average CMD solution using a 15 Gyr, [Fe/H]−1.5 isochrone is shown in the top panels. The final solution for a best-fitting CMD realization using a 10 Gyr, [Fe/H]=−1.6 CMD isochrone is shown in the bottom panels. The final solution (bottom row) has a smaller σ_{Fe} and smaller dependence on EP, wavelength, or reduced EW than the original solution.
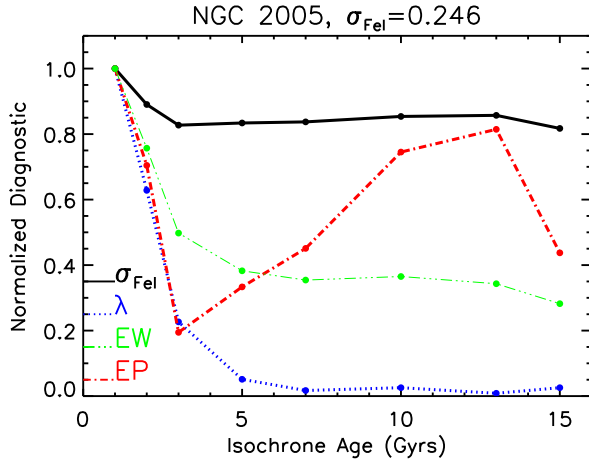
Figure 11. Same as Figure 3 for NGC 2005. Best solutions are found for ages >5 Gyr.
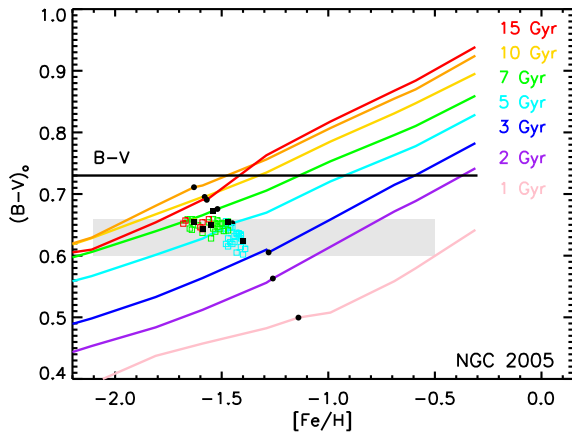
Figure 12. Same as Figure 7 for NGC 2005.

the integrated $B-V$ of a cluster when comparing it to the $(B-V)_0$ of the synthetic CMDs. However, while blue HB stars may be important for matching the $B-V$, cooler and redder stars continue to be more important for deriving self-consistent, stable [Fe/H] solutions. Moreover, our tests for sampling uncertainties are adequate to determine whether significant flux from cool AGB stars is necessary for a stable [Fe/H] solution. Despite the issues discussed for NGC 2005, we find that the [Fe/H] is well determined and is within ~ 0.1 dex of [Fe/H]=−1.6 over the $5-15$ age range found for the best-fitting CMD solutions.

4.4.3. *NGC 1916*

NGC 1916 is the most massive old cluster in the LMC training set ($M_V^{tot} = -8.96$), and we have observed a significant fraction ($\sim$60%) of the total flux. For that reason, we do not expect that sampling uncertainties will have a large impact on our solution. Nevertheless, we follow the same analysis procedure as for NGC 2019 and NGC 2005 for clarity and to demonstrate the impact of sampling uncertainties on an old, well-sampled cluster.

In Figure 14 we show the normalized Fe line diagnostics for the self-consistent average CMD solutions. Like NGC 2019 and NGC 2005, we find that the diagnostics for NGC 1916 are generally best for ages between 5 and 15 Gyrs. The Fe I lines result in solutions of [Fe/H]~ -1.5, with a best σ_{Fe}=0.259, which is comparable to the result for NGC 2005, but higher than that for NGC 2019. The 15 Gyr solution shows a fairly significant dependence of [Fe/H] with wavelength, a small dependence of [Fe/H] with reduced EW, and negligible dependence of [Fe/H] with EP.

As for NGC 2005, Olsen et al. (1998) observed a significant number of blue HB stars in NGC 1916, although their analysis of the HST CMD was hampered by differential reddening, so a precise age, [Fe/H], and $E(B-V)$ were not determined. We are in a unique position to determine an accurate [Fe/H] and age for NGC 1916 because we create synthetic CMDs to represent the cluster
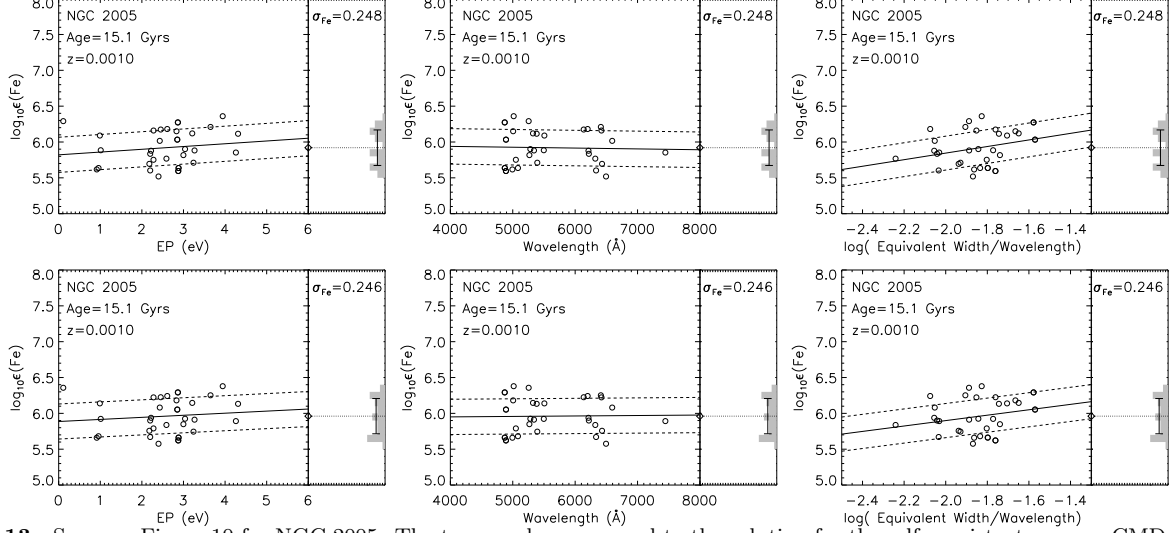
Figure 13. Same as Figure 10 for NGC 2005. The top panels correspond to the solution for the self-consistent average CMD solution for a 15 Gyr, [Fe/H]= −1.5 isochrone, and the bottom panels correspond to the solution for the best-fitting CMD realization from a 15 Gyr, [Fe/H]=−1.5 isochrone. The solution shown in the bottom panels has a smaller σ_{Fe}, and reduced [Fe/H] dependence on wavelength, EP, and reduced EW than the original solution.
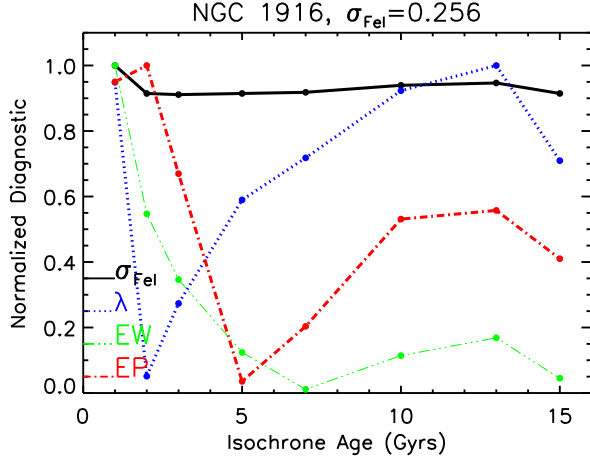
Figure 14. Same as Figure 3 for NGC 1916. Best solutions are found for ages >5 Gyrs.
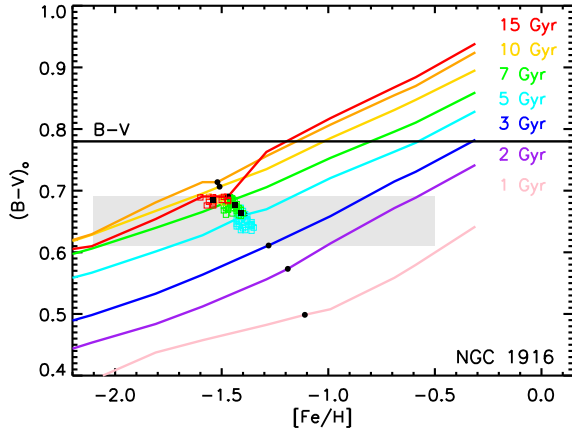
Figure 15. Same as Figure 7 for NGC 1916.

populations and are therefore not sensitive to differential reddening effects. We find that the reddening corrected $B − V$ color (Pessev et al. 2008) is inconsistent with the color of the 10 and 13 Gyr average CMD solutions, as shown in Figure 15. Because of the uncertainty in the $E(B − V)$ and the effect of blue HB stars, we test CMD realizations with a wide range in age and $(B−V)_0$ as we did for NGC 2005. CMD realizations with self-consistent [Fe/H] and marginal improvement in the diagnostics are found for ages of 5, 7 and 15 Gyrs. The most stable solutions have the same [Fe/H] as the average CMD solutions, and nearly identical $(B − V)_0$. This means that the stellar population for NGC 1916 was already well constrained using our original technique. In Figure 16 we show the original 15 Gyr average CMD solution, as well as the best-fitting solution from the 15 Gyr CMD realizations. The latter shows a slightly smaller σ_{Fe}, and slightly smaller dependence of [Fe/H] with wavelength and reduced EW than the original solution.

In summary, we find the best-fitting solutions for NGC 1916 have ages of 5 to 15 Gyrs, and a well-constrained [Fe/H]∼ −1.5. The fact that we cannot substantially improve the diagnostics by allowing for statistical fluctuations and a large range in $(B − V)_0$ suggests that any mismatch between the observed $B − V$ and the synthetic CMD $(B − V)_0$ could simply be due to a deficit of blue HB stars in the isochrones. In any case, both the preferred CMD population and the metallicity of NGC 1916 are well determined from our analysis. This is an important demonstration of the utility of our method for determining the properties of GCs affected by differential reddening, which are otherwise difficult to study using other means.

4.5. Results: Intermediate Age Clusters

We have tested our analysis method on two LMC clusters with ages of ∼1-2 Gyr. Even without a priori knowledge of the cluster ages, it is immediately apparent using our original technique that these clusters are better matched by CMDs with ages <5 Gyrs. As soon as this
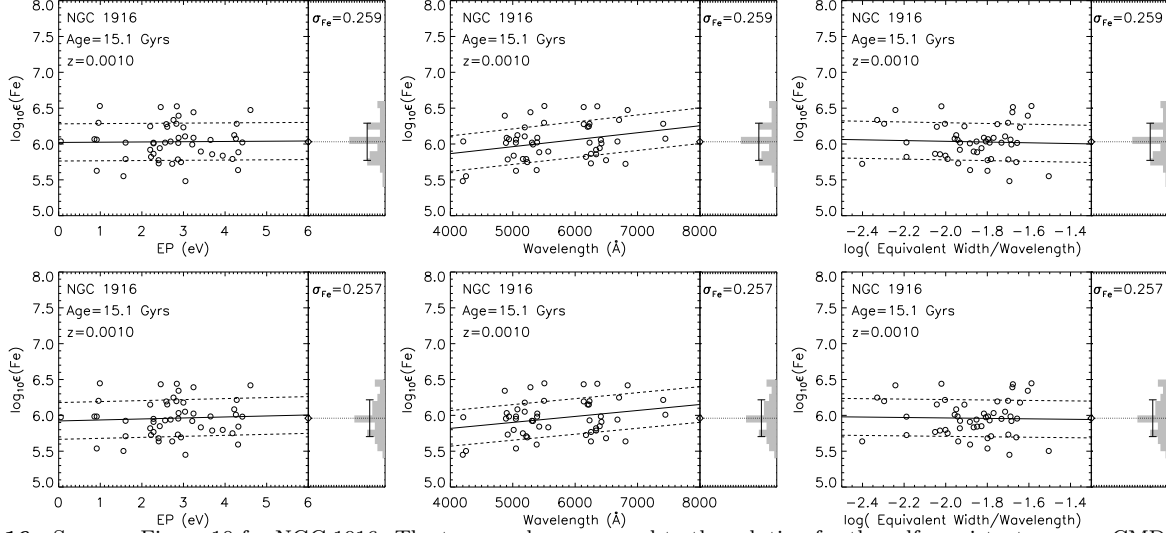
Figure 16. Same as Figure 10 for NGC 1916. The top panels correspond to the solution for the self-consistent average CMD solution for a 15 Gyr, [Fe/H]= −1.5 isochrone, and the bottom panels correspond to the solution for the best-fitting CMD realization from a 15 Gyr, [Fe/H]=−1.5 isochrone. The solution in the bottom panels has a smaller $\sigma_{\rm Fe}$ than the original solution.

is apparent, we use a finer grid of ages for our synthetic CMDs between 0.5 Gyr and 5 Gyr because significant changes in the CMD stellar populations can occur on much shorter timescales (0.5-1 Gyr) than they do for old, >5 Gyr CMDs. For the initial synthetic CMD grid, we use isochrones with ages of 0.5, 0.7, 1.0, 1.25, 1.5, 1.75, 2.0, 2.5, 3.0, 3.5, 5.0, 7.0, and 10 Gyr. We discuss the determination of the best-fit CMDs below.

It is especially important to evaluate the effect that sampling uncertainties can have on the age and abundance solutions for the intermediate age clusters. This is because they are both ∼2 Gyr in age, and therefore rapidly evolving, and because they are the least luminous, least massive, clusters in both the LMC and MW training sets, and therefore the most likely to suffer from statistical fluctuations in a small number of luminous stars. At a fixed total luminosity a 1 Gyr cluster has fewer, but more massive, more luminous, stars than a 10 Gyr cluster (e.g., see Brocato et al. 1999).

4.5.1. NGC 1718

NGC 1718 is the least massive cluster in the training set ($M_V^{\rm tot} \sim -6.5$), and is estimated to have an age of ∼2 Gyr (Kerber et al. 2007). The mean [Fe/H] solutions we derive for the grid of synthetic CMDs are shown in Figure 17, and the diagnostics for the self-consistent CMDs for each age are shown in Figure 18. The best $\sigma_{\rm Fe}$=0.324, which is significantly larger than the $\sigma_{\rm Fe}$ we obtain for any of the old clusters in the sample. However, even though the $\sigma_{\rm Fe}$ is large, it can clearly be seen in Figure 18 that all of the diagnostics are consistently better for the younger ages than they are for the older ages. This is the clearest demonstration to date that our abundance analysis method and the Fe I lines alone can be used to constrain cluster age.

We next investigate the limits we can place on the age of the cluster using this method, and whether we can successfully identify an age that is consistent with the age determined from resolved star photometry. Figure 18 shows that the minimum in $\sigma_{\rm Fe}$ occurs at 0.7 to 1.25 Gyrs, and that there is a corresponding minimum in the
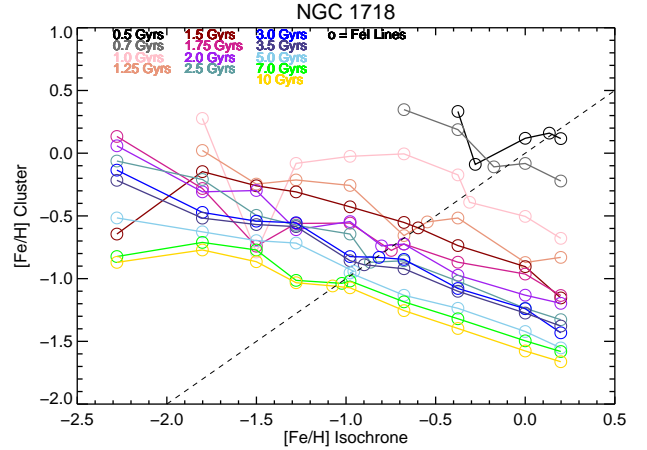

Figure 17. Same as Figure 2 for NGC 1718. Additional ages for the grid of synthetic CMDs for intermediate age clusters are shown by the labeled colors.

Fe I slope with EP and some indication of a minimum in Fe I slope with EW at these ages. However, while there is some indication of a preferred solution in the appropriate age range around 1 Gyr, the full range from 0.5 to 1.25 Gyr gives acceptable solutions. The 1 Gyr solution, with [Fe/H]∼ −0.4, has a small dependence of [Fe/H] with EP, but a significant dependence of [Fe/H] with both wavelength and reduced EW. This suggests that this CMD is a poor match to the true CMD of the cluster. Again, we next explore how incomplete sampling may play a role.

In Figure 19 we show the histogram of $(B-V)_0$ for 100 CMD realizations of a $M_V^{\rm tot}$=−6.5 cluster, which corresponds to the total flux of NGC 1718 (Kerber et al. 2007). Also shown is the histogram for CMD realizations for 23% of a $M_V^{\rm tot}$=−6.5 cluster, which corresponds to the fraction of NGC 1718 we have observed. The larger spread in $(B-V)_0$ of the CMD realizations in Figure 19 when compared to that for NGC 2019 in Figure 4 demonstrates that statistical stellar population fluctuations are a greater issue for NGC 1718. It is also clear from the
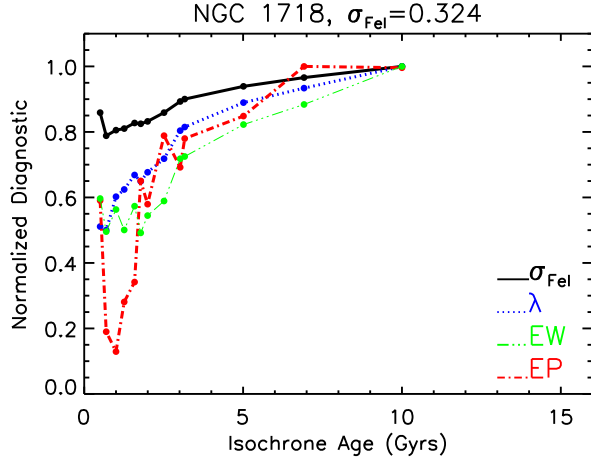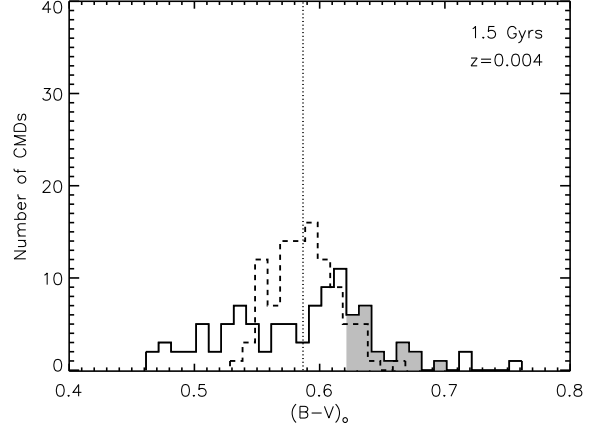
Figure 18. Same as Figure 3 for NGC 1718. The best solutions are found for ages of 0.7−1.25 Gyrs.

Figure 19. Histogram of integrated $(B-V)_0$ color for 100 CMD realizations of a 1.5 Gyr, z=0.004 ([Fe/H]=−0.66) isochrone. Solid black line shows the histogram for a population where the total flux in stars has been normalized to 23% of a $M_V^{\rm tot}=-6.5$ cluster, which is appropriate for our integrated light spectrum of NGC 1718. Dashed black line shows the histogram for a population normalized to 100% of a $M_V^{\rm tot}=-6.5$ cluster. CMDs with $(B-V)_0$ color consistent with the observed, reddening-corrected $B-V$ of NGC 1718 are shaded in gray. The large spread of $(B-V)_0$ in the solid line histogram is an indication that our observations of NGC 1718 are significantly affected by sampling incompleteness.

comparison of the two histograms for NGC 1718 in Figure 19 that the sampling uncertainties are significantly exacerbated by the incomplete sampling of our observations. It is particularly worrisome that the peak is hard to distinguish for the less luminous CMD realizations.
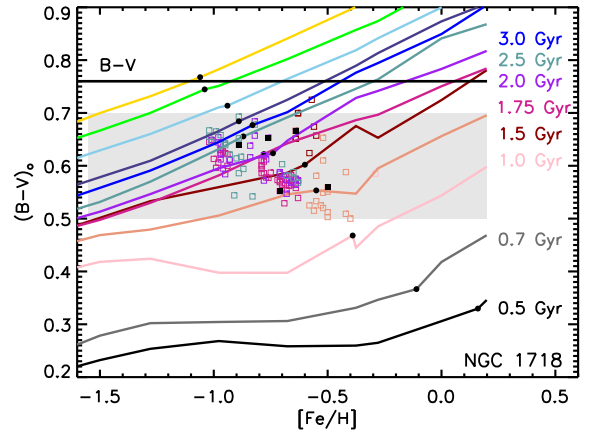
For NGC 1718, the large spread in $(B-V)_0$ is due to a combination of its significantly smaller luminosity, its young age, and the incomplete sampling of the observations. We are especially interested in evaluating the effect of its young age, as this will be most relevant to future work on unresolved clusters. It will be impossible to disentangle the uncertainties due to the age of NGC 1718 from the uncertainties due to our observations, but this means this is a worst case scenario for future work on unresolved clusters.

We create CMD realizations for NGC 1718 with ages and [Fe/H] in the range 1 to 2.5 Gyr and −0.98 to −0.26, and include isochrones at the interpolated [Fe/H] solutions from the average CMDs. The CMDs result in a wide range of [Fe/H] solutions, ranging from [Fe/H]~ -2 to [Fe/H]~ 0. This is a result of fairly drastic fluctuations in luminous giant stars, which both cause the large scatter in $(B-V)_0$ seen in Figure 19 and have a large impact on the Fe I EWs. Fortunately, this means that it is easier to use the Fe lines to identify CMD realizations that are viable solutions. For NGC 1718 we are able to narrow down the possible CMD realizations from >1000 to $\sim$120 by applying our usual requirement that the solutions be self-consistent, and that they have colors consistent with the cluster's observed properties. We include CMD realizations with 0.5< $(B-V)_0$< 0.7 for abundance analysis, which is highlighted by the shaded gray region in Figure 20. The upper limit of this range corresponds with the observed, reddening corrected $B-V$ of NGC 1718. We extend the lower limit of the $(B-V)_0$ range to include more CMD realizations with ages of 1 to 1.5 Gyr, which have bluer colors. We search a wider parameter space because of the significant trends in the original [Fe/H] solutions, and because Figure 18 suggests that the diagnostics at these ages are generally better. We note that even with a lower limit of $(B-V)_0$=0.5, it is pretty clear from Figure 20 that CMDs with ages <1.0 Gyr can be ruled out based on the observed $B-V$.

In Figure 21 we show the Fe I diagnostics for the CMD

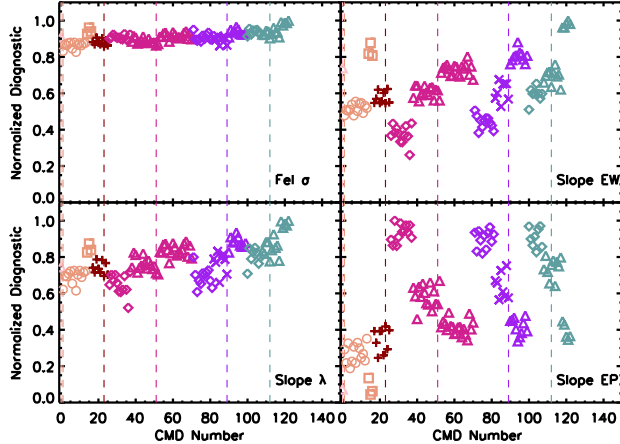**Figure 20.** Same as Figure 7 for NGC 1718. Colors are the same as in Figure 17. Shaded gray region corresponds to the range in $(B-V)_0$ allowed for the subset of CMD realizations used for abundance analysis.

realizations that have self-consistent [Fe/H] solutions, ordered first by increasing age and then by increasing [Fe/H] for each age. This figure shows that the $\sigma_{\rm Fe}$ tends to get larger with increasing age, as was found for the average CMDs in Figure 18, which implies that the younger ages are generally better solutions. We pick the solution that best minimizes all of the diagnostics for each age, while no one solution ideally minimizes all diagnostics at once. We find that the best-fitting CMD realization at each age has the same [Fe/H] as the original average CMD solution, which implies that in this case incomplete sampling is not adding significant uncertainty to the best-fitting [Fe/H], despite the sampling concerns discussed above.

After narrowing down the possible solutions from $\sim$120

**Figure 21.** Same as Figure 8 for NGC 1718. Colors are the same as in Figure 17. Younger ages are overall better solutions.

Figure 22. Same as Figure 18, except the 1.25-2.5 Gyr solutions have been replaced by the solutions for the best-fitting CMD realization at these ages. The best solutions are found for ages of 1−2.5 Gyr.

self-consistent CMD realizations to 5 solutions, one for each age, we compare these 5 solutions to the 7 average CMD solutions for the other ages in the grid. The diagnostics for these final 12 solutions are shown in Figure 22. We find that the case for an age of ∼1 Gyr is a little stronger than it was from Figure 18, due to an improvement in the σ_{Fe}, and that the other diagnostics are more closely correlated with this improvement. However, while the 1 to 1.25 Gyr solutions are the most stable overall, the differences between the solutions with ages between 1 to 2.5 Gyr are still small. Therefore, our final age constraint for NGC 1718 is 1 to 2.5 Gyr. This is a narrower range in age than we are generally able to constrain for old clusters, but because NGC 1718 is young, the stellar population changes considerably over this 2.5 Gyr timescale. Accordingly, the [Fe/H] solution is less constrained than for older clusters in the training set, although the solutions for the older clusters spanned a larger range in age. Explicitly, the 1.0 Gyr solution has [Fe/H]=−0.39, and the 2.5 Gyr solution has [Fe/H]=−0.89. To convey this range of possible solutions in age and corresponding abundance, we average the two [Fe/H] results and quote an uncertainty due to the age solution, σ_{age}, of ±0.25 dex.

To give a more qualitative impression of the difference between the original solution and the final solutions given above, in Figure 23 we compare the individual diagnostics for the average CMD solution with an age of 1.25 Gyr, compared to the best-fitting CMD realization with an age of 1.25 Gyr. The most significant improvement in the bottom panels when compared to the top panels is a reduced σ_{Fe}. Because there is still a significant dependence of [Fe/H] with EP, wavelength, and reduced EW, it is clear that our best-fitting stellar population is still not an ideal match to the true population of the cluster.

In summary, the analysis of NGC 1718 demonstrates that we are able to distinguish between clusters that are ∼1 Gyr in age from clusters that are >5 Gyr in age using our abundance analysis method. We are able to confidently constrain the age of NGC 1718 to a range of 1−2.5 Gyr using the stability of the [Fe/H] solution and the observed integrated color, albeit with a larger [Fe/H] uncertainty than for older clusters. Our final abundance constraint is [Fe/H]=−0.64, with an uncertainty due to
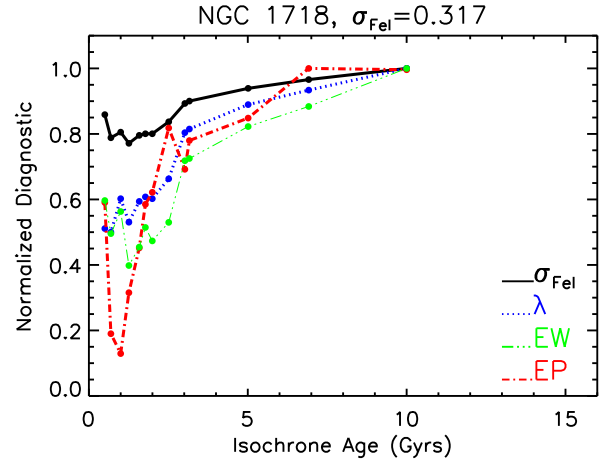
the age of $\sigma_{age} = \pm 0.25$ dex. The final error analysis is summarized in §5. As discussed above, the larger uncertainty in [Fe/H] could be refined with higher quality data and more complete sampling. While sampling uncertainties can cause a large spread in $(B - V)_0$, we are able to constrain a small subset of solutions by requiring self-consistency in the [Fe/H] solution. In the case of NGC 1718, we are able to slightly improve on the stability of the [Fe/H] solution by allowing for sampling uncertainties.
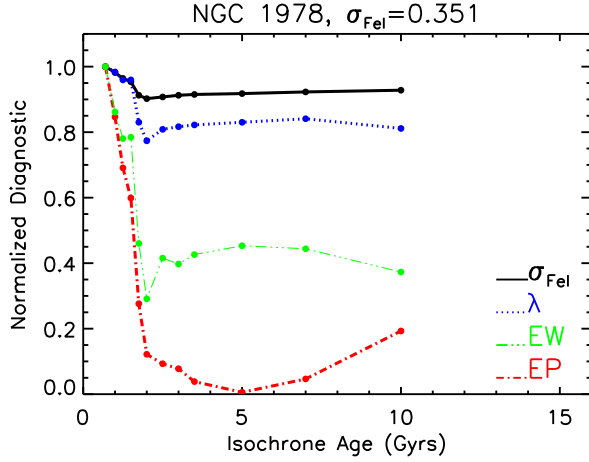
4.5.2. *NGC 1978*

The second intermediate age cluster in the LMC training set, NGC 1978, has an age of ∼2 Gyr and is more massive ($M_V^{tot} \sim -7.7$) than NGC 1718. Similar to NGC 2005, the S/N of the NGC 1978 spectrum is lower than for most of the other clusters in our MW and LMC training sets. We measure EWs for only 36 clean, reasonably unblended Fe I lines, whereas we typically measure 50−100 Fe I lines for clusters with high S/N data. The best solution has σ_{Fe}= 0.351, which is larger than the σ_{Fe} for NGC 1718, as well as the σ_{Fe} for the old clusters in the LMC training set. The low S/N makes NGC 1978 particularly difficult to analyze.

We calculate the [Fe/H] solutions for the same grid of isochrones as NGC 1718, but note that the average CMDs with ages of 0.5 Gyrs result in solutions with [Fe/H] > +0.5, which is outside the range of isochrones and stellar atmospheres used in our analysis and so are not considered further here. We show the normalized diagnostics for the self-consistent, average CMDs of the other 7 ages in Figure 24. In the case of NGC 1978, we find that the diagnostics show that the worst solutions have ages between 0.7 to 1.25 Gyrs. The solutions with ages >1.5 Gyr are of comparable quality, although there is some indication from the EP diagnostic that solutions with ages >7 Gyr are also unfavorable. The solutions with ages of 1.5 to 7 Gyr show a moderate dependence of [Fe/H] with both EP and reduced EW, and a significant dependence of [Fe/H] with wavelength. These diagnostics imply that the stellar populations are a poor match to the cluster.

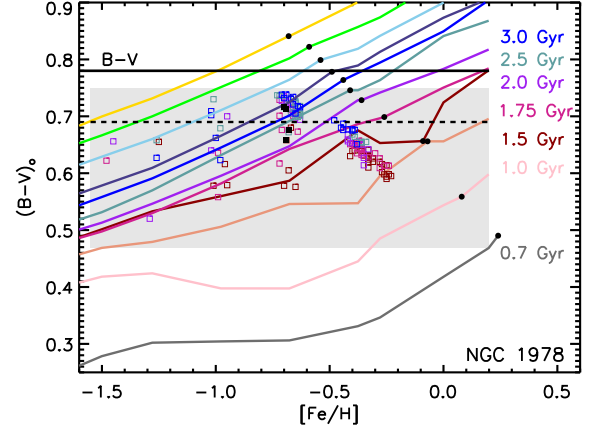We estimate that we have only observed 5−10% of the
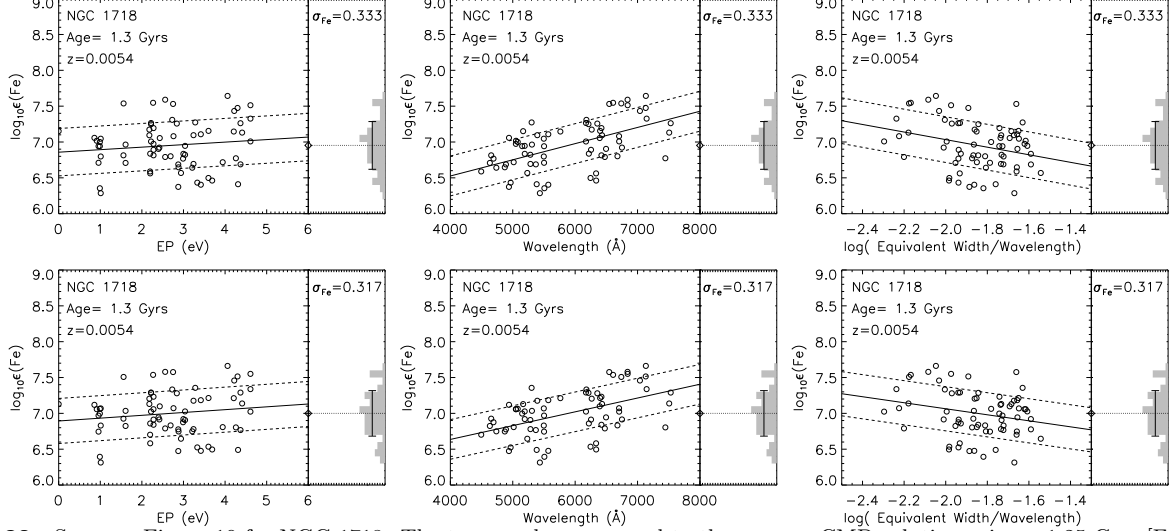
Figure 23. Same as Figure 10 for NGC 1718. The top panels correspond to the average CMD solution using a 1.25 Gyr, [Fe/H]=−0.55 isochrone, and the bottom panels correspond to the best-fitting CMD realization using a 1.25 Gyr, [Fe/H]=−0.55 isochrone. The solution in the bottom panels has a smaller $\sigma_{\rm Fe}$ and slightly smaller [Fe/H] dependence on EP, wavelength, and reduced EW.

Figure 24. Same as Figure 3 for NGC 1978. Best solutions are found for ages >1.5 Gyr.

Figure 25. Same as Figure 7 for NGC 1978. Colors are the same as in Figure 17. The shaded gray region corresponds to the range in $(B-V)_0$ allowed for the subset of CMD realizations used for abundance analysis.

total flux of NGC 1978 in the scanned region, which means that incomplete sampling is a significant issue. The synthetic CMDs for NGC 1978 have ∼4,000 stars, whereas a cluster with $M_V^{\rm tot}\sim -7.7$ would have ∼76,000 stars in the synthetic CMDs if we had observed 100% of the total flux. As in the case of NGC 1718, the synthetic CMDs for NGC 1978 have significantly less than 30,000 stars.
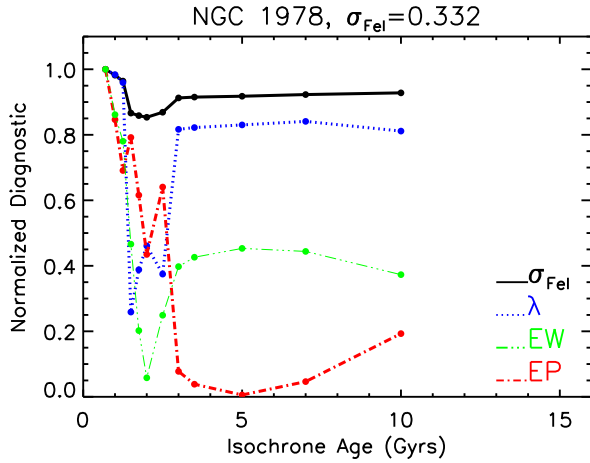
We create CMD realizations for ages of 1.5 to 3 Gyr and [Fe/H]= −1.5 to [Fe/H]= 0 to see if we can find a population that results in a more stable [Fe/H] solution. Like NGC 1718, for NGC 1978 we find that we are able to eliminate the majority of the possible CMD realizations using the self-consistency of the Fe lines. Out of these >3000 solutions, we only keep a subset of ∼150 CMD realizations that satisfy the requirement $0.47 <(B-V)_0< 0.75$. This is a fairly large range in $(B-V)_0$, and is chosen to include both the $E(B-V)$=0.09 of Mucciarelli et al. (2007) and the significantly larger value of $E(B-V)= 0.25$ from the catalog of Pessev et al. (2008). This $(B-V)_0$ requirement is

highlighted by the shaded gray area in Figure 25, where it can be seen that the average CMD solutions with ages >3 Gyr have $(B-V)_0$ colors inconsistent with this requirement. Moreover, from Figure 25 there is some justification for eliminating the average CMDs with ages >5 Gyr from consideration for a best-fitting solution because they have redder colors than the observed $B-V$.

We show the diagnostics for the subset of ∼150 self-consistent solutions in Figure 26, where it can be seen that all four Fe diagnostics show similar, correlated behavior with age and metallicity. We pick one best-fitting solution for each age (5 total), and compare the normalized diagnostics to the solutions for the other ages in Figure 27. From Figure 27 it appears clearer that there is a preferred age for NGC 1978 between 1.5 and 2.5 Gyr. There is significant improvement in the $\sigma_{\rm Fe}$, and a much smaller dependence of [Fe/H] on wavelength and reduced EW when compared to the average CMD solutions in Figure 24, although a dependence of [Fe/H] on EP and wavelength is still present. The difference be-
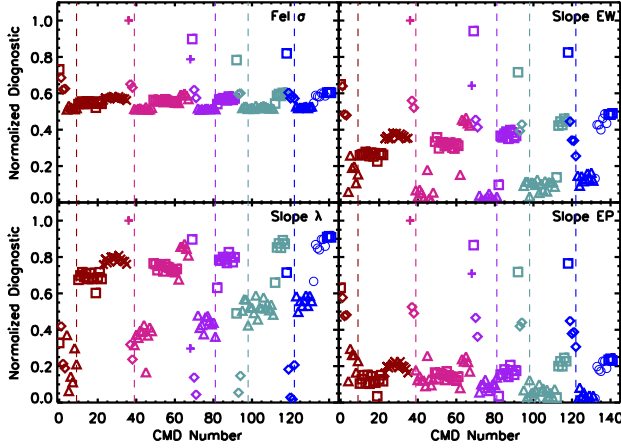
Figure 26. Same as Figure 21 for NGC 1978. Colors are the same as in Figure 17. Diagnostics are strongly correlated with both age and metallicity.

Figure 27. Same as Figure 24, except the solutions at ages of 1.5−2.5 Gyr have been replaced by the solutions for the best-fitting CMD realization at these ages. The best solutions are found for ages of 1.5−2.5 Gyr.

tween the best-fitting 2.5 Gyr CMD realization and the original averaged 2.5 Gyr CMD can be seen most clearly in Figure 28, where we compare the individual diagnostics.

Interestingly, we find that all of best-fitting CMD realizations for NGC 1978 have [Fe/H]~ -0.7, regardless of the age. The solution for NGC 1978 is therefore much better constrained than for NGC 1718. Note that this is also much more metal-poor than the solution obtained from the average CMDs. Comparing with the original solution, we find that the main difference is that the CMD realizations that allowed for partial sampling of the CMD have flux in much cooler AGB stars than the original solutions. This is further evidence that we are able to tell whether significant flux in cool AGB stars is needed in the synthetic CMDs by using the Fe I diagnostics. We also find that the best-fitting CMD realizations have $0.66 < (B-V)_0 < 0.72$, which corresponds to $0.07 < E(B-V) < 0.12$. This range is very consistent with the $E(B-V) = 0.09$ derived by Mucciarelli et al. (2007) from their very deep HST CMD, and supports the use of

this method to provide independent constraints on the $E(B-V)$ of unresolved clusters as done in Colucci et al. (2009).

In summary, the mean solution for NGC 1978 using the best-fitting CMD realizations with ages of 1.5 to 2.5 Gyr is [Fe/H]=-0.74, with $\sigma_{\mathrm{age}} = \pm 0.05$. Although the line-to-line scatter for the Fe abundance is also high, it is likely that it can be explained by the low S/N of the data. Like NGC 1718, we find that the best-fitting solutions for NGC 1978 show pretty significant dependence of [Fe/H] on EP and wavelength. However, unlike the case of NGC 1718, for NGC 1978 we find the [Fe/H] has only a weak dependence on age within the preferred age range, despite the low quality of the data and large standard deviation of the Fe lines.

These two clusters are very interesting illustrations of our method at intermediate ages. However, the two clusters are very different from each other. Given the data quality and that we only have two clusters in the intermediate age range, it is impossible to determine if the difficulties we encounter in finding an accurate stellar population match for these clusters is due to broader, generic problems in the isochrones at these ages. Along those lines, we note that there is still some debate over the presence or degree of convective overshooting needed in the input physics of the isochrones in order to match the observed CMDs of young clusters, which we discuss further in §5.1 (e.g. Pietrinferni et al. 2004; Mucciarelli et al. 2007). There are also many open questions as to the modeling of AGB star evolution and mass loss on the RGB, both of which can have a particularly significant effect on the integrated properties of clusters in this age range (e.g. Cordier et al. 2007; Girardi et al. 2000; Gallart et al. 2005). A more extensive training set of high quality integrated light spectra of clusters in this age range is clearly needed to begin to address these questions.

4.6. *Results: Young Clusters*

There are four young clusters in the LMC training set, which have ages < 1 Gyr. Like for the intermediate age clusters, it is immediately apparent using our original technique that these clusters are best matched by the youngest CMDs in our grid, and so we add synthetic CMDs with ages between 30−300 Myr to the analysis.

In the following sections we present the analysis for NGC 1866, NGC 1711 and NGC 2100. The remaining cluster, NGC 2002, has an estimated age of $\sim$15 Myrs (Elson 1991). Note that the youngest age in the grid of isochrones we currently employ for our analysis is 30 Myr. While we are able to measure EWs for NGC 2002 (as reported in Table 4), the solutions for synthetic CMDs with ages between 30 Myrs and 1 Gyr do not converge at self-consistent values of [Fe/H]. Indeed this cluster appears to be beyond the reach of our current technique, and so we do not discuss NGC 2002 further in this work.

4.6.1. *NGC 1866*

NGC 1866 is a relatively massive ($M_V^{\mathrm{tot}} \sim -9$), well-studied cluster, with an age of 100−200 Myr (e.g. Testa et al. 1999; Brocato et al. 2003). From the reasonably high S/N spectra for NGC 1866 we are able to measure 49 Fe I lines. We find a line-to-line scatter for
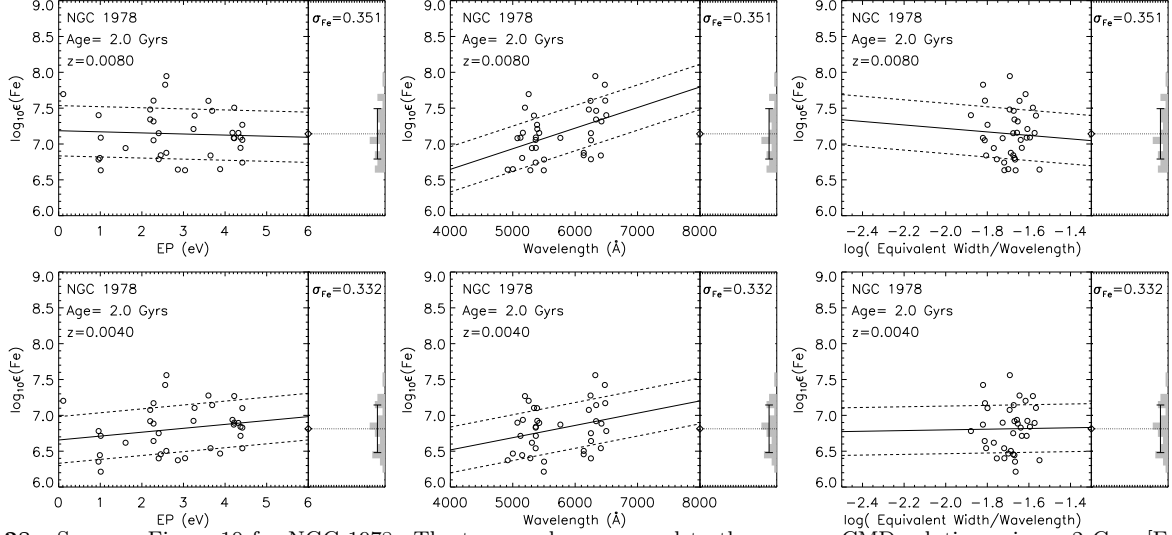
Figure 28. Same as Figure 10 for NGC 1978. The top panels correspond to the average CMD solution using a 2 Gyr, [Fe/H]=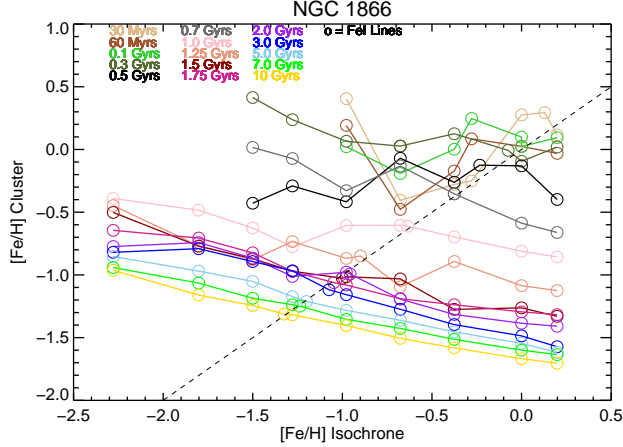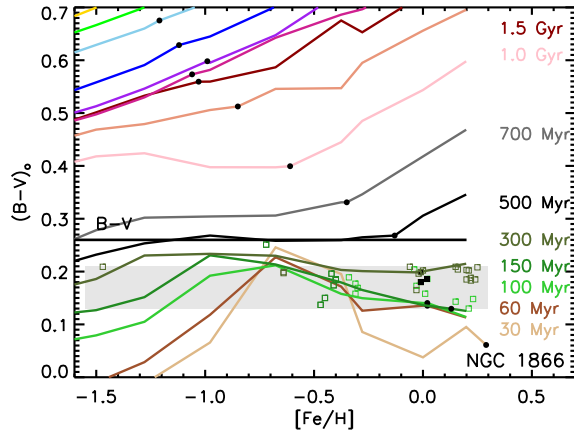−0.38 isochrone, and the bottom panels correspond to the best-fitting CMD realization using a 2 Gyr, [Fe/H]=−0.66 isochrone. The solution in the bottom panels has a smaller σ_{Fe}, and smaller [Fe/H] dependence on wavelength and reduced EW.

Figure 29. Same as Figure 2 for NGC 1866. Additional CMDs with ages <0.5 Gyr are shown by the labeled colors.
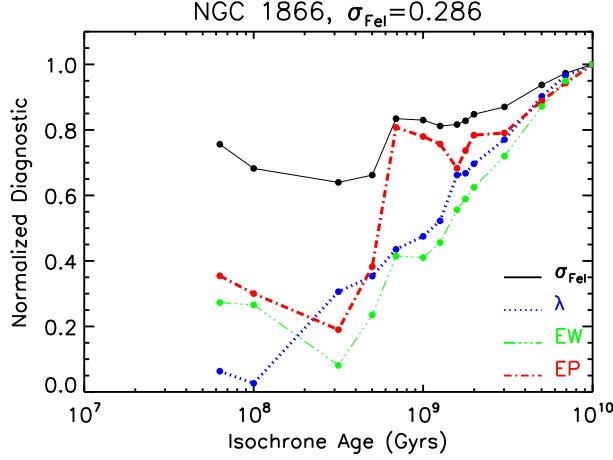

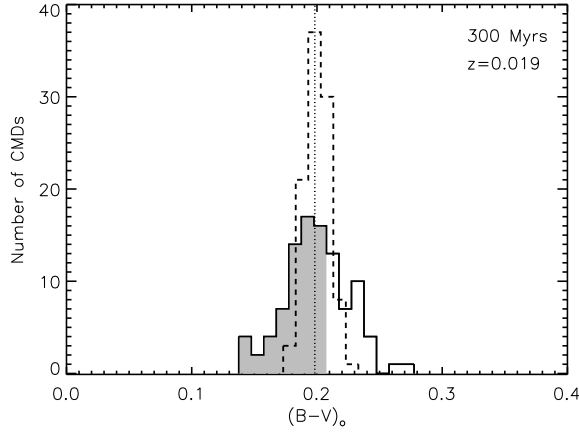**Figure 30.** Same as Figure 7 for NGC 1866. Colors are the same as in Figure 29.

the Fe I abundance that is comparable to that of the old clusters ($\sigma_{Fe} \sim 0.244$), and significantly smaller than that of the intermediate age clusters, which makes NGC 1866 a valuable test case for our abundance analysis methods.

We derive mean [Fe/H] values for the full grid of synthetic CMDs, which are shown in Figure 29. The [Fe/H]$_{cluster}$ solutions for synthetic CMDs with ages younger than 150 Myr deviate from the behavior of the [Fe/H]$_{cluster}$ of the older CMDs, which generally result in monotonically decreasing output [Fe/H]$_{cluster}$ with increasing input [Fe/H]$_{iso}$. This behavior is due to the stellar atmospheres over-compensating the Fe abundance to match the observed Fe EWs when the input [Fe/H]$_{iso}$ is lower than the real abundance, or under-compensating when the input [Fe/H]$_{iso}$ is too high. For synthetic CMDs with old ages, the stellar populations generally change slowly and smoothly with increasing metallicity, which leads to the smooth change in derived [Fe/H]$_{cluster}$. For synthetic CMDs with ages <150 Myr, the temperatures of core He-burning, luminous super-giants not only vary significantly on short timescales, but are also very sensitive to metallicity (e.g. Chiosi et al. 1992; Brocato & Castellani 1993; Brocato et al. 1999). For this grid of isochrones, the averaged, synthetic CMDs with ages <150 Myr and [Fe/H]=−1 to −0.3 contain supergiants at cooler temperatures than CMDs at other metallicities at the same age. Because the cooler supergiants have stronger Fe I features, the derived [Fe/H] tend to be lower, which is seen in Figure 29.

The temperature of the luminous supergiants also significantly affects the integrated colors of the synthetic CMDs. In Figure 30, we show the behavior of the integrated $(B - V)_0$ for the grid of isochrones as a function of [Fe/H]$_{iso}$. As expected, the youngest synthetic CMDs with [Fe/H]=−1 to −0.3 have redder $(B - V)_0$ colors than CMDs at other metallicities (note the "bump" in $(B - V)_0$ at −0.7 <[Fe/H]< −0.5 for the 30−100 Myr age isochrones). A more subtle point that can be seen in Figure 30 is that there is a complicated $(B - V)_0$-metallicity-age degeneracy for synthetic CMDs with ages <150 Myr. We will return to this point below.
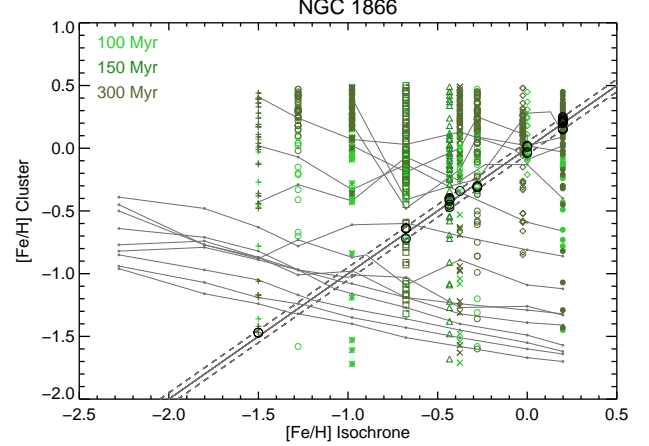
Figure 31. Same as Figure 3 for NGC 1866. Best solutions are for ages of 100−300 Myr.

Figure 33. Same as Figure 29, with the addition of the Fe I abundance results for the CMD realizations of NGC 1866. Colors of the points denote the same ages as Figure 29. Only CMD realizations consistent with the observed $B − V$ color of NGC 1866 are shown. Black circles on the solid black line denote CMD realizations that satisfy the self-consistent criterion $[Fe/H]_{iso}=[Fe/H]_{cluster}$. Only a small number of the possible CMD realizations have self-consistent $[Fe/H]$ solutions.

Figure 32. Histogram of integrated $(B − V)_0$ color for 100 CMD realizations of a 300 Myr, z=0.019 ($[Fe/H]=0$) isochrone. Solid black line shows the histogram for a population where the total flux in stars has been normalized to 14% of a $M_V^{tot}= −9$ cluster, which is appropriate for our integrated light spectrum of NGC 1866. Dashed black line shows the histogram for a population normalized to 100% of a $M_V^{tot}= −9$ cluster. CMDs with $(B − V)_0$ color consistent with the observed, reddening-corrected $B − V$ of NGC 1866 are shaded in gray.

The complex behavior of the $[Fe/H]_{cluster}$ solutions in Figure 29 hints that constraining the $[Fe/H]$ of clusters with ages <1 Gyr may be difficult. For NGC 1866, the self-consistent synthetic CMDs with younger ages (and hotter stars), tend to have more metal-rich $[Fe/H]$ solutions. In Figure 31 we show the diagnostics for the 14 self-consistent CMD solutions for the initial grid. It is very clear from the Fe I line diagnostics alone that a young age for NGC 1866 is preferred. Specifically, the most stable $[Fe/H]$ solutions for NGC 1866 are found at ages of 100−500 Myrs. Note that this independent age constraint using our abundance analysis method is very consistent with the observed $B − V$=0.26 from Pessev et al. (2008).

In view of the earlier discussion of the importance of luminous supergiants for clusters in this age regime, one would expect sampling uncertainties to be important here. However, in the case of NGC 1866, the orig-

inal, average CMD solutions for ages of 100−300 Myr are very stable and show only a very slight dependence of $[Fe/H]$ with EP and wavelength. Because these solutions are very stable already, we are unlikely to find an improved CMD realization. Nevertheless, it is interesting to ask what range in age or $[Fe/H]$ can produce a similarly good CMD when stochastic sampling is considered. To that end, the dashed line in Figure 32 shows a histogram of the integrated $(B − V)_0$ of 100 CMD realizations created for an isochrone with an age of 300 Myr, and $[Fe/H]=0$, which is consistent with the properties we derive for NGC 1866. The CMD realizations that make up the dashed line histogram have been normalized to the total flux of a $M_V^{tot}\sim −9$ cluster. It can be seen in Figure 32 that a cluster with $M_V^{tot}\sim −9$ is massive enough that the range of $(B − V)_0$ is small ($\sim$0.05 mag) because the CMDs are not significantly impacted by statistical fluctuations in the number and properties of the supergiant stars. Similarly, even though we estimate that we have only observed 14% of the total flux of NGC 1866, we find that CMD realizations normalized to 14% of the flux of a $M_V^{tot}\sim −9$ cluster are still so well-populated that the spread in $(B − V)_0$ is only a little larger ($\sim$0.1 mag), and comparable to that for the better sampled old clusters in the training set. The histogram for 100 CMD realizations normalized to the observed region of NGC 1866 is shown by the solid line in Figure 32.

Fluctuations in $(B − V)_0$ tend to be larger at lower metallicities (see Figure 30), especially for clusters with young ages. Although it appears that NGC 1866 is massive enough that incomplete sampling is not a major issue, it is important to establish if acceptable CMD realizations exist at lower metallicities and whether they result in more stable $[Fe/H]$ solutions. For this test, we create CMD realizations with ages of 100−300 Myr, and $[Fe/H]=−1.5$ to +0.2. In determining a range in $(B − V)_0$ for the self-consistent CMD realizations, we note that NGC 1866 is well-studied and there are several estimates of the $E(B − V)$ that are consistently in the
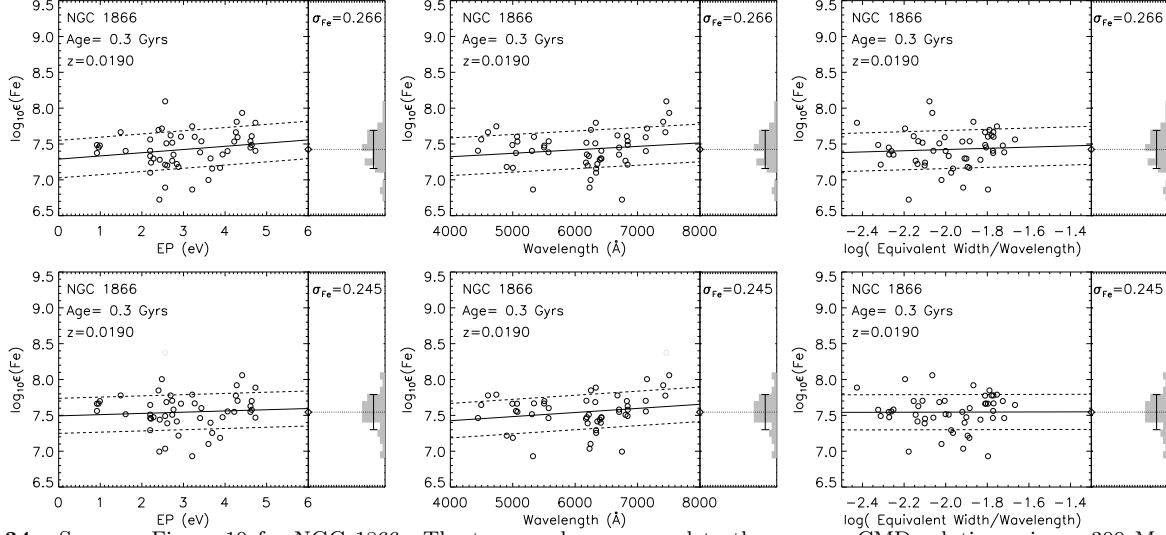
Figure 34. Same as Figure 10 for NGC 1866. The top panels correspond to the average CMD solution using a 300 Myr, [Fe/H]=0 isochrone, and the bottom panels correspond to the best-fitting CMD realization using a 300 Gyr, [Fe/H]=0 isochrone. The solution in the bottom panels has a smaller $\sigma_{\rm Fe}$.
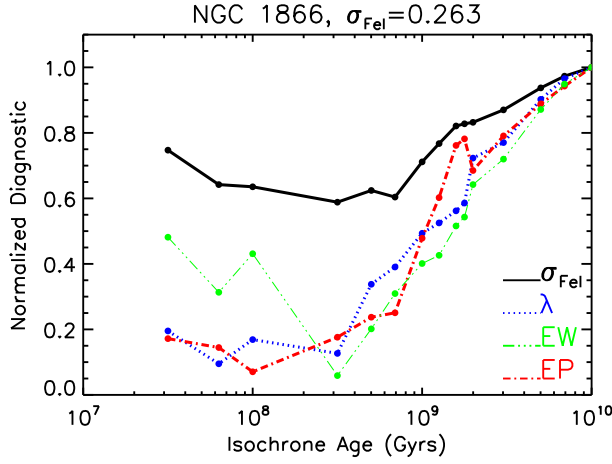
Figure 35. Same as Figure 31, except the solutions at ages of 100−300 Myr have been replaced by the solutions for the best-fitting CMD realization at these ages. Best solutions are for ages of 100-300 Myr.

range of 0.06 to 0.13. The $(B-V)_0$ requirement that we use includes this range of $E(B-V)$, as shown by the shaded gray region in Figure 30.

As found for the intermediate age clusters, for NGC 1866 the spread in $(B-V)_0$ leads to a large spread in [Fe/H]$_{\rm cluster}$. The solutions range from [Fe/H]=−1.7 to > +0.5. We show the results for the CMD realizations with ages of 100, 150, and 300 Myr in Figure 33; compared to the original average CMD solutions for reference. Out of the large number of CMD realizations, only ∼50 result in self-consistent solutions and satisfy the $(B-V)_0$ requirement (see those falling on the diagonal line in Figure 33). Because so many of the possible CMD realizations do not satisfy the [Fe/H] self-consistency requirement, we can conclude that for young clusters our analysis method is very successful in picking out a small range of viable CMD realizations from a large set of CMD possibilities, just as discussed for the intermediate age clusters in § 4.5. This is due to the sensitivity of the Fe line EWs to the temperature of the luminous supergiants.

From the ∼50 possible self-consistent CMD realizations, we pick one best-fitting CMD realization for each age by minimizing the Fe I line diagnostics. We find that solutions with [Fe/H]∼0 are the most stable solutions overall, just as was found from the original average CMD solutions. These solutions have a smaller $\sigma_{\rm Fe}$ than the original average CMD solutions, and small improvements in the EP, wavelength, and reduced EW diagnostics. A comparison of the individual diagnostics for the 300 Myr average CMD solution and the best-fitting 300 Myr CMD realization is shown for reference in Figure 34. In Figure 35 we show the normalized diagnostics for the solutions with ages of 100−500 Myr compared to the average CMD solutions at other ages. From Figure 35 we derive a final age constraint for NGC 1866 of 100−300 Myr. The range of [Fe/H] for the 100−300 Myr solutions results in a mean of [Fe/H]=+0.05 and $\sigma_{\rm age} = 0.06$, which is comparable to the standard error in the mean of the Fe I abundance.

4.6.2. NGC 1711

NGC 1711 is estimated to have an age of 50 Myr (Dirsch et al. 2000), and is less massive than NGC 1866 ($M_V^{\rm tot} - 8.3$). Our analysis of NGC 1711 is hampered by low S/N spectra and poor sampling (∼16%). We are only able to measure ∼25 reasonably clean Fe I lines, and find a high line-to-line scatter of $\sigma_{\rm Fe} \sim 0.45$. These difficulties mean that the constraints we can make from our abundance analysis are limited, but we find the general trends are consistent with those of NGC 1866.

We find that the self-consistent [Fe/H] solutions appear at [Fe/H]∼ −0.9 for synthetic CMDs with ages <300 Myrs, as shown in Figure 36. These solutions fall into the region of $(B-V)_0$-metallicity space that is very sensitive to the evolution of cool supergiants. These solutions also imply that NGC 1711 is reasonably metal-poor for its young age, although the high scatter in the Fe I abundance solution must be kept in mind. However, there is also some indication from Figure 36 that the 30 Myr CMD solutions near solar metallicity are also close to a self-consistent [Fe/H]. The large jumps in output [Fe/H]
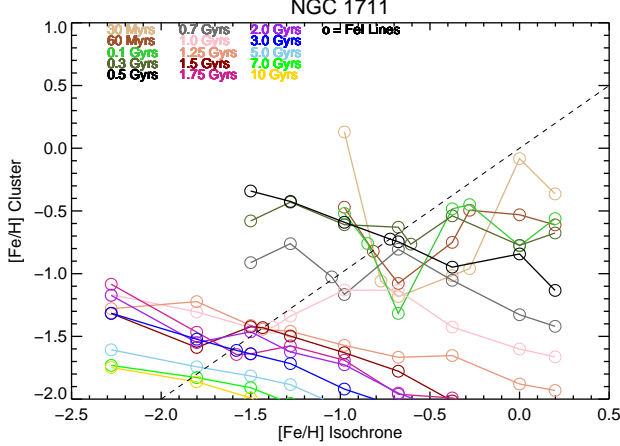
Figure 36. Same as Figure 2 for NGC 1711.
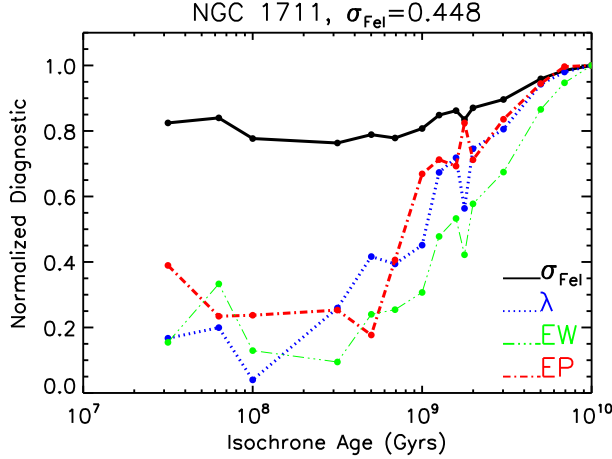
Figure 37. Same as Figure 3 for NGC 1711. Best solutions are for ages of <300 Myr.

Figure 38. Histogram of integrated $(B-V)_0$ color for 100 CMD realizations of a 60 Myr, z=0.004 ([Fe/H]=−0.66) isochrone. Solid black line shows the histogram for a population where the total flux in stars has been normalized to 16% of a $M_V^{\rm tot}=-8.3$ cluster, which is appropriate for our integrated light spectrum of NGC 1711. Dashed black line shows the histogram for a population normalized to 100% of a $M_V^{\rm tot}=-8.3$ cluster. CMDs with $(B-V)_0$ color consistent with the observed, reddening-corrected $B-V$ of NGC 1711 are shaded in gray. The range in $(B-V)_0$ for the CMD realizations is very large, demonstrating that sampling uncertainties are a big concern.

indicate that sampling uncertainties are having an impact on the synthetic CMDs and the [Fe/H] solution, as well.

Although the [Fe/H] solutions are not ideal in terms of absolute quality, we are still able to evaluate the relative quality of the solutions for different ages. We find that, like NGC 1866, the normalized diagnostics for the self-consistent solutions for each age clearly suggest the best solutions are at the youngest ages, as seen in Figure 37. For NGC 1711, we find that the solutions imply an age <300 Myr. This is further evidence that the Fe lines are powerful diagnostics for determining ages of young clusters, and it suggests that with high quality data our abundance analysis method could be used to put tighter constraints on age and [Fe/H] of ~50 Myr clusters that are sufficiently massive and well-sampled.

We repeat the exercise of creating CMD realizations covering the range of interest in age and [Fe/H], primarily to evaluate if we can see evidence for better solutions at more metal-rich abundances.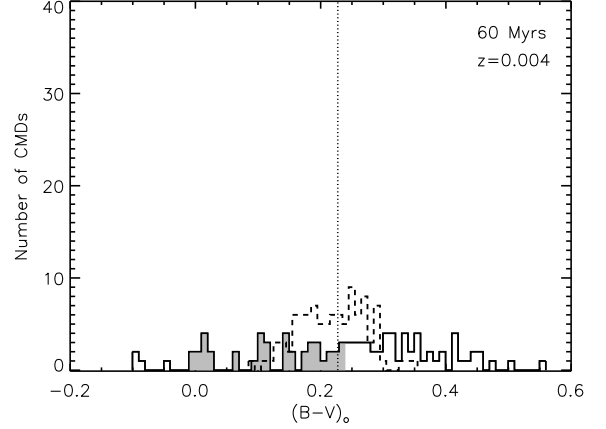 For a comparison to the older clusters in the training set, we show the $(B-V)_0$ histogram of 100 CMD realizations created for a $M_V^{\rm tot}=-8.3$, 60 Myr cluster, like NGC 1711, by the dashed lines in Figure 38. We note that the

$(B-V)_0$ scale in Figure 38 is bigger than for the histograms shown for other clusters in this work, because the range in $(B-V)_0$ for the CMD realizations is larger. This is most apparent from the solid line histogram, which is made from CMD realizations normalized to the total flux of 16% of a $M_V^{\rm tot}-8.3$ cluster, which corresponds to the fraction of NGC 1711 we have observed. The range of $(B-V)_0$ for the CMD realizations in this histogram is ~0.6 mag, significantly higher than the ~0.1 mag discussed for NGC 1866. Figure 38 underscores the fact that it is crucial that young clusters are very luminous and well-sampled when observed for integrated light analyses (e.g. Brocato et al. 1999).

We next explore the range of solutions that can be obtained from the CMD realizations for NGC 1711. We allow the subset of CMD realizations used for abundance analysis to have a wide range in color ($0.0<(B-V)_0<$ 0.3), due to large uncertainties in the observed $B-V$ and $E(B-V)$ of Pessev et al. (2008) and Dirsch et al. (2000). Because the stellar populations change rapidly at the youngest ages, we also refine the age grid for the CMD realizations to include additional ages of 40, 50, and 80 Myr. While in general we do not find that the self-consistent CMD realizations offer significant improvements over the average CMD solutions, it is clearer that the best solutions are for ages of 60-300 Myr. The solutions at the best fit ages cover a range in [Fe/H] of −0.66 to −0.97, so we quote an abundance of [Fe/H]=−0.82 with an uncertainty due to the assumed age of $\sigma_{\rm age}=$ 0.15 dex. The individual diagnostics for the best-fitting 60 Myr CMD realization are shown in Figure 39, where the large line-to-line scatter can be fully appreciated.

In conclusion, although the [Fe/H] solution for NGC 1711 has significant uncertainties, the general trends from the analysis are very similar to that of NGC 1866. This suggests that in the future it may be possible to obtain even tighter constraints for ~50 Myr clusters that
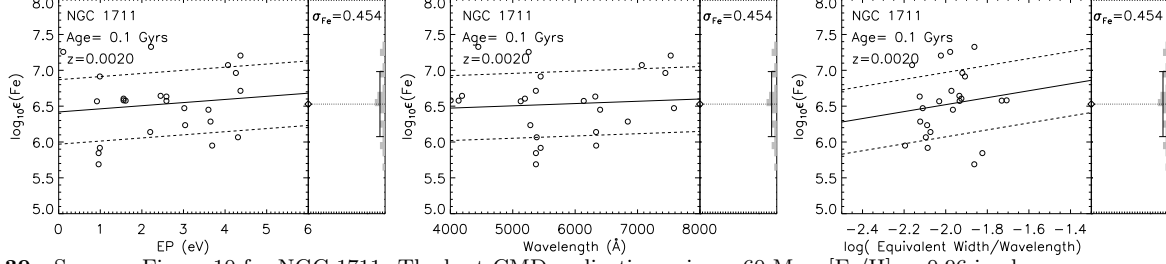
Figure 39. Same as Figure 10 for NGC 1711. The best CMD realization using a 60 Myr, [Fe/H]=−0.96 isochrone.
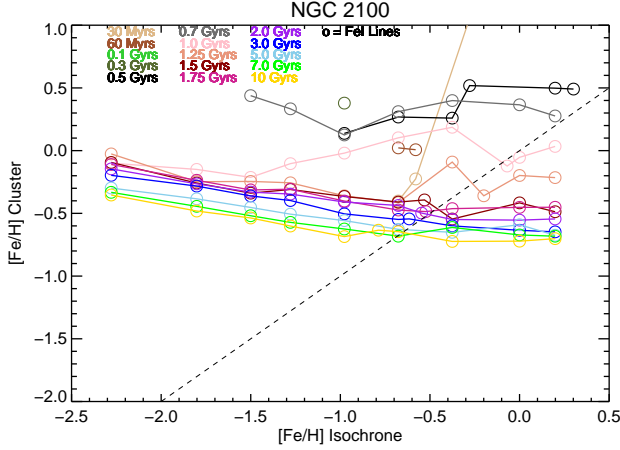
Figure 40. Same as Figure 2 for NGC 2100.

Figure 41. Same as Figure 3 for NGC 2100. Best solutions are for ages of <40 Myr.

are more massive and better sampled than NGC 1711.

4.6.3. *NGC 2100*

The youngest cluster in the LMC training set for which we can constrain abundances is NGC 2100, which is estimated to have an age of 15 Myr (Elson 1991), and $M_V^{tot} \sim -8.8$. Our best solution is from 33 clean Fe I lines and has an uncertainty of σ_{Fe}=0.32, which is lower than the line-to-line scatter for NGC 1711 but larger than for NGC 1866.

NGC 2100 is sufficiently young and metal-rich that we are unable to find solutions that converge at self-consistent [Fe/H] for the average CMDs with ages between 30 Myr−300 Myr. The average CMD solutions for NGC 2100 are shown in Figure 40. Although the average CMD solutions do not converge at self-consistent [Fe/H], there is some indication that there may be possible solutions for an age of 30 Myr and [Fe/H]> −0.7, given the spread we expect from incomplete sampling effects. To determine if self-consistent solutions exist, we create CMD realizations for ages of 30, 40, and 100 Myr and −0.66 <[Fe/H]< +0.0 in the sampling uncertainty tests. We use an additional color constraint of −0.13 < $(B-V)_0$< 0.22, which covers the range in observed $B-V$ and $E(B-V)$ from Table 1.

We find that a handful of CMD realizations with [Fe/H]∼ 0 result in self-consistent solutions, and that all of the self-consistent solutions have ages <40 Myr. These solutions have diagnostics that are significantly better than any self-consistent solutions with ages >500 Myr, as can be seen in Figure 41. The individual diagnostics for the best-fitting 40 Myr, [Fe/H]=0 CMD realization are shown in Figure 42. This solution has a negligible

dependence of [Fe/H] with EP, a small dependence of [Fe/H] with reduced EW, and a significant dependence of [Fe/H] with wavelength.

In summary, even though our grid of synthetic CMDs does not probe ages as young as that determined for NGC 2100 from resolved photometry, we are in fact able to put an upper limit on the age of NGC 2100 of 40 Myr using the Fe lines and our abundance analysis method. Our final abundance constraint for NGC 2100 is [Fe/H]= −0.03; this abundance can be considered a lower limit given our age constraint.

The analysis of all three young clusters in the LMC training set demonstrates that using our abundance analysis method, we can obtain very tight constraints on the age and abundance of massive clusters with ages of of ∼ 50 to 500 Myr, and limits on the age and abundance for clusters as young as 10 Myr. We see evidence for the significant impact of luminous supergiants on both the integrated $(B-V)_0$ colors and the derived [Fe/H] abundances. As was the case for the intermediate age clusters, for the young clusters it is the sensitivity of the [Fe/H] solution to luminous, cool stars that facilitates strong constraints on age and metallicity from high resolution integrated light spectra. By allowing for statistical fluctuations in the synthetic CMDs, we are able to reduce the σ_{Fe} of the original solutions and improve the [Fe/H] stability with EP, wavelength, and reduced EW. Moreover, we find that with high quality data, the self-consistency and stability of the [Fe/H] solution can break the $(B-V)_0$-metallicity degeneracy seen in Figure 30.

4.7. *Summary of Results*
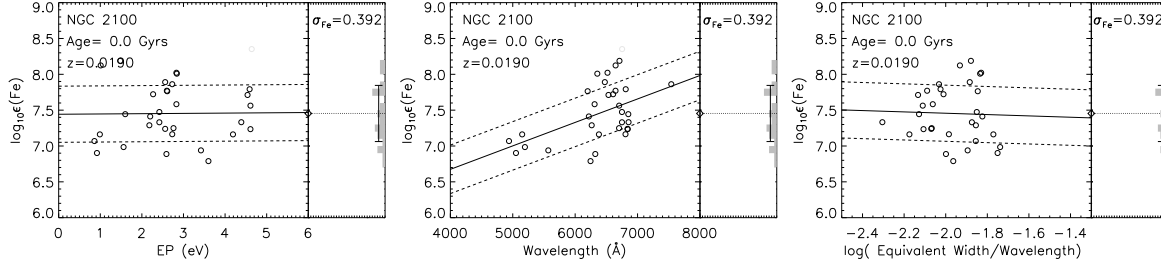
Figure 42. Same as Figure 10 for NGC 2100. The best CMD realization using a 40 Myr, [Fe/H]=0 isochrone.

We have measured the ages and determine [Fe/H] abundances for eight of the nine clusters in the LMC training set (NGC 2019, 2005, 1916, 1718, 1978, 1866, 1711, and 2100), as listed in Table 6. With this sample of clusters, we have demonstrated the ability to measure both a wide range in metallicity ($-1.5 <$[Fe/H]$< +0.0$) and age (40 Myr to 12 Gyr) using a single abundance analysis technique. Four of these clusters (NGC 1916, 1718, 1711, and 2100) have no prior measurements of [Fe/H] from high S/N, high resolution spectroscopy.

In the analysis of each cluster, we have discussed two sources of uncertainty in our measurement of [Fe/H]. The first is the line-to-line statistical scatter in the abundance of individual Fe lines, σ_{Fe}, and the second is the uncertainty in [Fe/H] due to the assumed age, σ_{age}. For a final uncertainty for each cluster, σ_{total}, we add the standard error in the mean of the Fe lines and the age uncertainty in quadrature, which we have listed in column 7 of Table 6. The standard error in the mean of the Fe lines is defined as $\sigma_{Lines} = \sigma_{Fe}/(N_{Lines}-1)$, where N_{Lines}, the number of measured Fe I lines for each cluster, is listed in column 3 of Table 6. An evaluation of systematic offsets is presented in §5.1.

5. DISCUSSION

In the first part of this section, we discuss additional sources of uncertainty in our analysis due to the isochrones used to construct synthetic CMDs. Next, we compare the results of the IL spectra analysis method to cluster properties previously determined with other methods. In § 5.3, we discuss the age-metallicity relationship derived for our training set LMC clusters.

5.1. *Other Sources of Uncertainty: Choice of Isochrones*

An important additional source of uncertainty is, of course, the physics and assumptions that went into the isochrones. For example, we determine whether to use scaled-solar or α-enhanced Teramo isochrones on a cluster-by-cluster basis, after evaluating each clusters' Ca, Si and Ti abundances (presented in Paper IV). In principle, the level of α-enhancement can have an effect on the derived age and [Fe/H], because α-enhanced stars have higher opacities, resulting in slightly stronger metal lines (Salaris et al. 1993; Pietrinferni et al. 2006). Because the Teramo isochrones only come in two extremes — [α/Fe]=+0.4 or +0.0 — a potential concern is that our [Fe/H] and age solutions could be affected by a mismatch in the α-enhancement of the isochrone and the true α-enhancement of the cluster.

Fortunately, because we explicitly measure the [α/Fe] ratio of each cluster, we can estimate the systematic offset in [Fe/H] that is due to a mismatch between the Ter-

amo isochrones and the true [α/Fe]. To estimate the systematic offset we derive solutions for our clusters with both of the values of the Teramo isochrones, and then interpolate an offset for each cluster based on the measured [α/Fe]. The final systematic error for each cluster, α_{offset}, is listed in the last column of Table 6.

We find that for the old clusters, the systematic offset is small, and is ≤ 0.03 dex in all three cases. This offset is always smaller than the statistical uncertainty in [Fe/H] due to the line-to-line scatter or assumed age of the older clusters. For the younger clusters, we also derive small errors of ~ 0.04 dex for all of the clusters with the exception of NGC 1718, for which we find an offset of $+0.15$ dex. This is not unexpected because this cluster already has a large uncertainty in the [Fe/H] value due to the assumed age. We are unable to derive an offset for the case of NGC 2100, because the α-enhanced isochrone solutions do not converge, as in most cases for the solar isochrones for this young cluster.

We can also evaluate whether the choice of scaled-solar or α-enhanced isochrones adds a significant uncertainty to our age constraints. In all cases, we find that our original age constraints are conservative enough that the choice of isochrones does not change our final solutions. This is, in fact, consistent with previous work on the effect of α-enhancement on age measurements using low resolution IL line index techniques. In this case, indexes with Balmer line absorption are typically used for age determinations, and at the same age and [Fe/H] an α-enhanced star has weaker Balmer lines than a scaled-solar star. This leads to younger inferred ages, which are typically different by ~ 3 Gyr for old populations and ~ 1 Gyr for intermediate age populations (e.g. Schiavon 2007). $1 - 3$ Gyr is well within our original constraints, moreover, metal lines are not nearly as sensitive to α-enhancement as the Balmer lines. Therefore, an additional strength in our analysis when compared to low resolution line index methods is that we can independently determine the age of a cluster with metal lines, without the additional complications of Balmer line age dating.

Another potential source of uncertainty in our choice of isochrones involves the treatment of convective overshooting in the cores of massive ($> 1.1 M_\odot$) stars. This work is the first high resolution integrated light abundance analysis where the treatment of convective overshooting is relevant, because for the first time we have a sample of young clusters containing massive stars. In this paper we chose to use the non-canonical Teramo isochrones, which include convective overshooting, because they were found to best reproduce the high quality photometry of NGC 1978 (Mucciarelli et al. 2007). How-

Table 6
IL spectra Age and Abundance Results

Cluster	Age (Gyrs)	[Fe/H][a]	N_{Lines}[b]	σ_{Lines}[c]	σ_{Age}	σ_{total}[d]	α_{offset}[e]
NGC 2019	>7	−1.61	49	0.03	0.04	0.05	−0.03
NGC 2005	>5	−1.50	34	0.04	0.05	0.06	−0.02
NGC 1916	>5	−1.48	50	0.04	0.07	0.08	<0.01
NGC 1718	1.0-2.5	−0.64	69	0.04	0.25	0.25	+0.15
NGC 1978	1.5-2.5	−0.74	36	0.06	0.05	0.08	+0.03
NGC 1866	0.10-0.30	+0.04	49	0.04	0.02	0.04	−0.04
NGC 1711	0.06-0.30	−0.82	25	0.09	0.15	0.17	+0.04
NGC 2100	<0.04	>−0.03	33	0.06	$\cdots$	0.06	$\cdots$

Note. — a. The [Fe/H] value is the average value of the solutions with ages listed in column 2, and uncorrected for the α_{offset} in column 8. b. N_{mLines} corresponds to the number of Fe I lines used in the abundance analysis for each cluster. c. The standard error in the mean of the [Fe/H] measurement is defined as $\sigma_{Lines} = \sigma_{Fe}/(N_{Lines}-1)$. d. The total statistical error is defined as $\sigma_{total} = \sqrt{\sigma_{Lines}^2 + \sigma_{Age}^2}$. e. α_{offset} is a systematic error due to a difference in the α-enhancement of the Teramo isochrones and the true α-enhancement of the cluster, as discussed in §5.1.

Table 7
Comparison of Canonical and
Non-Canonical Isochrones

Cluster	Non-Canonical [Fe/H]	Canonical [Fe/H]
NGC 1718	−0.64	−0.70
NGC 1978	−0.74	−0.60
NGC 1866	+0.04	−0.19
NGC 1711	−0.82	−0.54
NGC 2100	>−0.03	> +0.03

ever, after this paper was submitted, Mucciarelli et al. (2010) measured detailed abundances of individual stars in NGC 1866 (age ∼150 Myr), and found a lower [Fe/H] than what we have found in our IL analysis. Because the non-canonical isochrones we have used have higher temperatures than the canonical isochrones, in the case of NGC 1866 we would in fact derive higher [Fe/H] solutions at ages of 100 to 300 Myrs with the non-canonical tracks than with the canonical tracks. If this is indeed the reason that our [Fe/H] for NGC 1866 is higher than that measured by Mucciarelli et al. (2010), then our analysis has extremely interesting implications for the long-standing convective overshooting debate in the literature (e.g. Testa et al. 1999; Barmina et al. 2002). Therefore, we have begun preliminary tests to evaluate the effect of convective overshooting on our [Fe/H] solutions, and present [Fe/H] estimates using the canonical isochrones for the intermediate age and young clusters in Table 7. We will present the full analysis of this interesting topic and conclusions on the most appropriate level of convective overshooting in an upcoming paper.

5.2. *Previous Estimates of Cluster Properties*

Our goal in this section is to look for broad consistencies or inconsistencies with previous results from a variety of techniques: high resolution spectra of individual stars, low resolution Ca II triplet (Ca T) spectroscopy, CMDs, Strömgren photometry, and low resolution line index methods. We note that, unlike for the MW training set clusters, there is only a subset of clusters in the LMC training set (NGC 2019, NGC 2005, NGC 1978, and NGC 1866) for which comparisons can be made to

abundances obtained from high resolution analysis of individual stars. However, even for these clusters it is important to keep in mind that many systematic uncertainties can arise due to choice of analysis methods, and that detailed abundances of stars determined by different authors typically do not agree to better than ±0.1 dex (see discussions in Gratton et al. 2004; Kraft & Ivans 2003). In addition to a handful of detailed abundances from individual stars, CMDs for all clusters are available in the literature, albeit of variable depth and quality. These CMDs have been used to constrain ages and estimate metallicities for the clusters, just as is done for clusters in the MW. Metallicity estimates from low resolution Ca T spectroscopy or line index methods exist for most of the clusters as well. Below, we summarize the previous estimates for ages and metallicities of the training set clusters compared to what we measure with high resolution abundance analysis. In addition, we compare our high resolution IL [Fe/H] results with previous measurements in Figure 43. Note that our IL abundances in Figure 43 have been corrected with the α_{offset} derived for each cluster. In addition, for the younger clusters, we show the anticipated shift in IL abundances when an analysis with a more appropriate treatment of convective overshooting is used.

NGC 2019. We obtain a measurement of [Fe/H]=−1.64 ± 0.05, which includes the α_{offset} as well as uncertainties due to line-to-line scatter and age. We derive an age of >7 Gyr. Johnson et al. (2006) measured detailed abundances for a sample of 3 RGB stars in NGC 2019 and found [FeI/H]=−1.37 ± 0.07 and a significantly higher [FeII/H]= −1.10 ± 0.16 from Fe II lines. Reasons for the offset in Fe I and Fe II abundances have been discussed profusely in Kraft & Ivans (2003) and Paper I and II. Olsen et al. (1998) estimate [Fe/H]=−1.23±0.15 from an HST WFPC2 CMD. Using low resolution Ca T spectroscopy of individual stars, Olszewski et al. (1991) estimate [Fe/H]=−1.8 ± 0.2, while Grocholski et al. (2006) find a more metal-rich [Fe/H]=−1.31. Beasley et al. (2002) find [Fe/H]=−1.43 ± 0.2 for NGC 2019 using low resolution IL spectra. This wide range in measurements from −1.8 <[Fe/H]< −1.10 is consistent with our measurement. Olsen et al. (1998) also derive an age of >12 Gyr by comparison the HST CMD to MW clusters and

the location of the HB, consistent with our age constraint.

NGC 2005. We obtain a measurement of [Fe/H]= -1.52 ± 0.06, with an age constraint of > 5 Gyr. As was the case for NGC 2019, Johnson et al. (2006) find significantly different abundances for Fe I and Fe II lines of [FeI/H]= -1.78 ± 0.09 and [FeII/H]= -1.31 ± 0.03. Olsen et al. (1998) find [Fe/H]= -1.35 ± 0.16 using an HST CMD. The metallicity estimate of Olszewski et al. (1991) from low resolution Ca T spectroscopy is more metal-poor than the CMD estimate, at [Fe/H]= -1.92 ± 0.2. The line index metallicity estimate is [Fe/H]= -1.45 ± 0.2 (Beasley et al. 2002). The range of these measurements is $-1.92 <$ [Fe/H] < -1.31, and is consistent with our result. Olsen et al. (1998) also find an old age of >12 Gyr for NGC 2005.

NGC 1916. We measure an abundance of [Fe/H]= -1.48 ± 0.08 and we are able to constrain the age to >5 Gyr. Olszewski et al. (1991) measured an abundance of [Fe/H]= -2.08 ± 0.2 using Ca T spectroscopy. Beasley et al. (2002) estimate [Fe/H]= -1.8 to -2.1 using various line indexes, which highlights the importance of high resolution abundances for GCs with moderate to low metallicities. These estimates of the metallicity of NGC 1916 are significantly lower than our measurement, but the greater uncertainties in low resolution techniques at lower metallicities must be kept in mind (see discussion in Colucci et al. 2009). While an HST CMD for NGC 1916 exists in Olsen et al. (1998), no detailed analysis of cluster properties was performed due to differential reddening. However, Olsen et al. (1998) note there is a blue horizontal branch present in the CMD, indicating that NGC 1916 is old (>10 Gyr), similar to our age constraint.

NGC 1718. We find [Fe/H]= -0.49 ± 0.25 and constrain the age of NGC 1718 to $1-2.5$ Gyr. Kerber et al. (2007) estimate [Fe/H]= -0.40 ± 0.10 using an HST CMD. With Ca T spectroscopy, Grocholski et al. (2006) find [Fe/H]= -0.80, and with line indexes, Beasley et al. (2002) find [Fe/H]= -0.98 to -1.12. This range of $-1.12 <$ [Fe/H] < -0.40 and the age of 2 ± 0.15 of Gyr Kerber et al. (2007) is consistent with our result that NGC 1718 is a relatively metal-poor intermediate age cluster. Our preliminary analysis shows that the canonical isochrones have a minor effect on the solution, and only lower the abundance by 0.06 dex.

NGC 1978. We obtain a measurement of [Fe/H]= -0.71 ± 0.08, with an age constraint of $1.5-2.5$ Gyr. There are two groups that have measured detailed abundances from individual RGB stars in NGC 1978. Ferraro et al. (2006) find [Fe/H]= -0.38 ± 0.07 from a sample of 11 stars, while Hill et al. (2000) find [Fe/H]= -0.96 ± 0.2 from 2 stars. The mean of these two studies is in good agreement with our result. Using low resolution Ca T, Olszewski et al. (1991) determine [Fe/H]= -0.42 ± 0.2, which is consistent with our result within the uncertainties. Mucciarelli et al. (2007) present a very deep HST ACS CMD of NGC 1978, and derive a best fit age of 1.9 ± 0.1 Gyr, but with an assumption about the metallicity based on high resolution spectroscopy of individual stars. We find that canonical isochrones may have a significant effect on the abundance we derive for NGC 1978, with an average offset of +0.14 dex. The positive offset would put our solu-
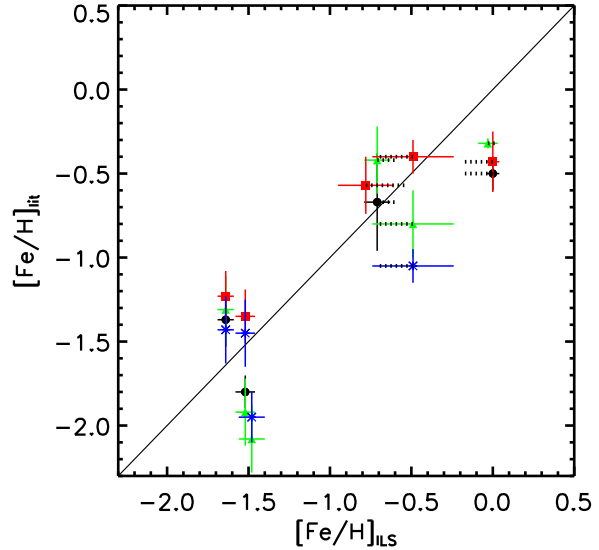
Figure 43. Comparison of previous metallicity estimates to IL abundance analysis results. Results from the literature for high resolution spectroscopy of individual stars, for photometric estimates, and for low resolution CaT measurements, for photometric estimates, and for low resolution line index methods are shown as black circles, green triangles, red squares, and blue stars, respectively. References for metallicities from the literature are discussed in § 5.2. Black dotted lines show the anticipated change in [Fe/H] when isochrones with more appropriate treatment of convective overshooting are used.

tion more in line with that of Ferraro et al. (2006) and Olszewski et al. (1991), and will be investigated further in a future paper.

NGC 1866. Our measurement is [Fe/H]= $+0.00 \pm 0.04$, and an age of 100 to 300 Myrs. Hill et al. (2000) find [Fe/H]= -0.50 ± 0.1 from a sample of 3 giant stars, and Mucciarelli et al. (2010) find [Fe/H]= -0.43 ± 0.04 from a sample of 14 stars. Using Strömgren photometry, Hilker et al. (1995) derive a metallicity for NGC 1866 of [Fe/H]= -0.43 ± 0.18, with the caveat that the calibration assumes that MW and LMC clusters have similar metallicities, which is not generally the case. Our result is more metal-rich than these other studies, however in §5.1 we discussed how the treatment of convective overshooting in the isochrones could be influencing our results. As shown in Table 7, preliminary results suggest that using the canonical Teramo isochrones in our analysis would lower the abundance to [Fe/H]= -0.19, closer to previous studies of individual stars. Testa et al. (1999) find an age of $100-200$ Myr for NGC 1866 from a deep, ground-based CMD, while from a HST CMD, Brocato et al. (2003) derive an age of $140-250$ Myr depending on assumptions about binary fractions and convective overshooting. Our age estimate is consistent with these results.

NGC 1711. We measure [Fe/H]= -0.78 ± 0.17, and constrain the age to a range of 60 to 300 Myr. Dirsch et al. (2000) derive an age of 50 Myr from a CMD, which is close to our constraint. Dirsch et al. (2000) find [Fe/H]= -0.57 ± 0.17 using Strömgren photometry, which is consistent with our result given the large uncertainties. We note that, like NGC 1866, we find pre-
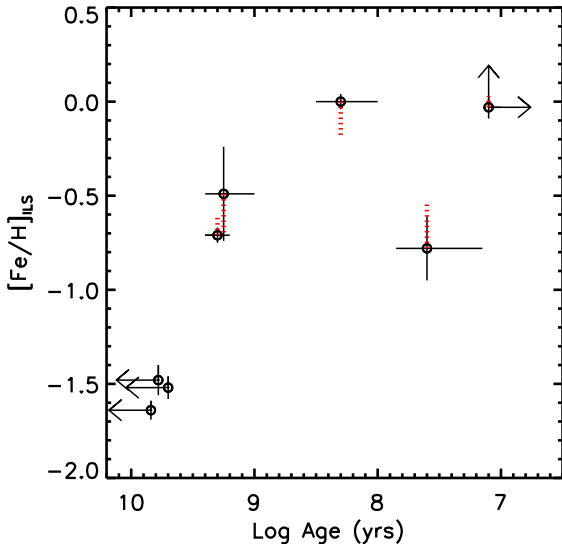
Figure 44. Age-metallicity relationship from IL abundance analysis for LMC training set clusters. Red dotted lines show the anticipated change in [Fe/H] when isochrones with more appropriate treatment of convective overshooting are used.

liminary evidence that the treatment of convective overshooting may impact our solution, and raise the abundance to [Fe/H]=−0.54, which would bring it closer to the result of Dirsch et al. (2000).

NGC 2100. We are able to put a lower limit on the metallicity of [Fe/H]=−0.03, and an upper limit on the age of 40 Myr. From medium resolution spectroscopy and spectral synthesis matching, Jasniewicz & Thevenin (1994) find a more metal-poor result of [Fe/H]= −0.32. While our measurement is significantly more metal-rich, it is impossible to evaluate systematic uncertainties between our technique and that of Jasniewicz & Thevenin (1994). We do not find evidence that our limit will change substantially if canonical isochrones are used in the analysis. To investigate this further, we will report follow-up high resolution spectroscopy of individual stars in NGC 2100 to look for possible systematic offsets from our technique. Jasniewicz & Thevenin (1994) find an age of 9 Myr, and Elson (1991) find 15 Myr, which are both consistent with our upper limit.

5.3. *Age-Metallicity Relationship*

In Figure 44 we show the age-metallicity relationship from our high resolution abundance analysis for the LMC clusters in our training set. The [Fe/H] values have been corrected with α_{offset}, and the possible shift due to isochrone choice is shown by red dotted lines for each cluster. In general, the more recently formed (younger) clusters have higher [Fe/H], as one would expect, and our results agree well with the age-metallicity relationship determined by Harris & Zaritsky (2009) and Carrera et al. (2008). However, even though this sample of LMC clusters is small, we find a small spread in [Fe/H] at constant age for clusters with ages of >10 Gyr and a larger spread for clusters with ages of ∼150 Myr, both of which are larger than the abundance uncertainties of the

individual clusters. This suggests that chemical enrichment across the LMC was inhomogeneous or that some clusters or gas may have been accreted from other merging satellites. The largest metallicity difference at a fixed age occurs for NGC 1866 and NGC 1711, at an age of ∼100 Myr. These clusters are on the outskirts of the LMC and separated from each other by several degrees on the sky, so this may be a result of accretion, poor mixing of the ISM, and/or infall of low metallicity gas. This is discussed further in Paper IV of this series, where we present ∼20 more element abundances for these LMC clusters to investigate the chemical enrichment and star formation history of the LMC in greater detail.

6. SUMMARY

We have analyzed a training set of clusters in the LMC using the high resolution IL abundance analysis method originally developed and tested on MW clusters in Paper I and Paper II. In this work we have tested the method on clusters with ages <10 Gyr for the first time, and developed a strategy to accommodate the effect of incomplete statistical sampling of CMD stellar populations. While this strategy is motivated by incomplete sampling in the training set clusters in particular, for which we have only observed a fraction of the stellar population due to the large spatial extent of the clusters on the sky, it is applicable without any a priori knowledge of a cluster's resolved stellar populations and can also be applied to distant extragalactic clusters. This is primarily important for low luminosity and young clusters, as their integrated properties are more sensitive to statistical fluctuations in the number of stars in short-lived, cool, luminous stages of stellar evolution.

Our IL abundance analysis of clusters with ages of 1−5 Gyr and <1 Gyr has demonstrated that clusters of these ages can be distinguished from old clusters using constraints derived from the Fe lines in the high resolution spectra alone. For intermediate age clusters we find that we can constrain ages to a ≤2.5 Gyr range, but that this range can result in a larger error on the derived abundances than typically found for old clusters. For the two intermediate age clusters in the training set we have found abundance solutions with higher scatter and less stability in [Fe/H] than generally found in the analysis of old clusters. This is likely due to low S/N data and poor statistical sampling, but it is possible that it is a systematic problem in the synthetic CMD populations at these ages. For the young clusters in the training set we have found that we can constrain ages to a 200 Myr range for a well sampled cluster with high S/N spectra, and in some cases can determine upper limits to ages and abundances for clusters with ages <30 Myr. Preliminary evidence suggests that the abundance solutions for young clusters could be sensitive to the input physics of the isochrones used to construct our synthetic CMDs.

The IL abundance analysis of >10 Gyr LMC clusters has demonstrated that even with low S/N data (∼ 40), 20 to 30 Fe lines are generally available for analysis, and that good constraints on the ages and abundances can be obtained with even a small number of lines. The analysis of NGC 1916 has shown that precise ages and abundances can be obtained for clusters with significant differential reddening.

In conclusion, we have demonstrated the utility of

the new high resolution IL spectra abundance analysis method to obtain tight age, abundance, and stellar population constraints on clusters spanning a large range in age from ∼50 Myrs to >10 Gyrs. Using this method, we have measured properties of LMC clusters spanning both a large range in age and a large range in [Fe/H] using a single, consistent technique. The age-metallicity relationship for this small set of LMC clusters suggests that the ISM of the LMC was not well mixed during all epics of star formation. Chemical abundances for an additional ∼20 elements will be presented in Paper IV, where we will investigate the chemical evolution history of the LMC in greater detail.

REFERENCES

Barmina, R., Girardi, L., & Chiosi, C. 2002, A&A, 385, 847

Beasley, M. A., Hoyle, F., & Sharples, R. M. 2002, MNRAS, 336, 168

Bernstein, R., Shectman, S. A., Gunnels, S. M., Mochnacki, S., & Athey, A. E. 2003, in Society of Photo-Optical Instrumentation Engineers (SPIE) Conference Series, Vol. 4841, Society of Photo-Optical Instrumentation Engineers (SPIE) Conference Series, ed. M. Iye & A. F. M. Moorwood, 1694–1704

Bernstein, R. A., Cameron, S., Colucci, J. E., & Mc William, A. 2011a, in preparation

Bernstein, R. A. & McWilliam, A. 2002, in IAU Symposium, Vol. 207, Extragalactic Star Clusters, ed. D. Geisler, E. K. Grebel, & D. Minniti, 739–+

Bernstein, R. A. & McWilliam, A. 2005, in Resolved Stellar Populations, ed. D. Valls-Gabaud & M. Chavez, Astronomical Society of the Pacific Conference Series

Bernstein, R. A., Prochaska, J. X., & Burles, S. 2011, in preparation

Bica, E., Claria, J. J., Dottori, H., Santos, Jr., J. F. C., & Piatti, A. E. 1996, ApJS, 102, 57

Brocato, E. & Castellani, V. 1993, ApJ, 410, 99

Brocato, E., Castellani, V., Di Carlo, E., Raimondo, G., & Walker, A. R. 2003, AJ, 125, 3111

Brocato, E., Castellani, V., Poli, F. M., & Raimondo, G. 2000, A&AS, 146, 91

Brocato, E., Castellani, V., Raimondo, G., & Romaniello, M. 1999, A&AS, 136, 65

Bruzual, G. & Charlot, S. 2003, MNRAS, 344, 1000

Cameron, S. A. 2009, PhD thesis, University of Michigan

Carrera, R., Gallart, C., Hardy, E., Aparicio, A., & Zinn, R. 2008, AJ, 135, 836

Castelli, F. & Kurucz, R. L. 2004, ArXiv Astrophysics e-prints

Chiosi, C., Bertelli, G., & Bressan, A. 1992, ARA&A, 30, 235

Colucci, J. E. 2010, PhD thesis, University of Michigan

Colucci, J. E., Bernstein, R. A., Cameron, S., & Mc William, A. 2011b, in preparation

Colucci, J. E., Bernstein, R. A., Cameron, S., Mc William, A., & Cohen, J. G. 2009, ApJ, 704, 385

Cordier, D., Pietrinferni, A., Cassisi, S., & Salaris, M. 2007, AJ, 133, 468

Dirsch, B., Richtler, T., Gieren, W. P., & Hilker, M. 2000, A&A, 360, 133

Elson, R. A. W. 1991, ApJS, 76, 185

Faber, S. M., Friel, E. D., Burstein, D., & Gaskell, C. M. 1985, ApJS, 57, 711

Faber, S. M. & Jackson, R. E. 1976, ApJ, 204, 668

Fagiolini, M., Raimondo, G., & Degl'Innocenti, S. 2007, A&A, 462, 107

Ferguson, J. W., Alexander, D. R., Allard, F., Barman, T., Bodnarik, J. G., Hauschildt, P. H., Heffner-Wong, A., & Tamanai, A. 2005, ApJ, 623, 585

Ferraro, F. R., Mucciarelli, A., Carretta, E., & Origlia, L. 2006, ApJ, 645, L33

Fischer, P., Welch, D. L., & Mateo, M. 1992, AJ, 104, 1086

Gallart, C., Zoccali, M., & Aparicio, A. 2005, ARA&A, 43, 387

Girardi, L., Bressan, A., Bertelli, G., & Chiosi, C. 2000, A&AS, 141, 371

Gratton, R., Sneden, C., & Carretta, E. 2004, ARA&A, 42, 385

Graves, G. J. & Schiavon, R. P. 2008, ApJS, 177, 446

Grocholski, A. J., Cole, A. A., Sarajedini, A., Geisler, D., & Smith, V. V. 2006, AJ, 132, 1630

Harris, J. & Zaritsky, D. 2009, AJ, 138, 1243

Harris, W. E. 1996, AJ, 112, 1487

Hilker, M., Richtler, T., & Gieren, W. 1995, A&A, 294, 648

Hill, V., François, P., Spite, M., Primas, F., & Spite, F. 2000, A&A, 364, L19

Jasniewicz, G. & Thevenin, F. 1994, A&A, 282, 717

Johnson, J. A., Ivans, I. I., & Stetson, P. B. 2006, ApJ, 640, 801

Kerber, L. O., Santiago, B. X., & Brocato, E. 2007, A&A, 462, 139

Kraft, R. P. & Ivans, I. I. 2003, PASP, 115, 143

Kroupa, P. 2002, Science, 295, 82

Kumar, B., Sagar, R., & Melnick, J. 2008, MNRAS, 386, 1380

Mackey, A. D. & Gilmore, G. F. 2003, MNRAS, 338, 85

McLaughlin, D. E. & van der Marel, R. P. 2005, ApJS, 161, 304

McWilliam, A. & Bernstein, R. A. 2008, ApJ, 684, 326

McWilliam, A., Preston, G. W., Sneden, C., & Shectman, S. 1995, AJ, 109, 2736

Meléndez, J. & Barbuy, B. 2009, A&A, 497, 611

Meynet, G. & Maeder, A. 2000, A&A, 361, 101

Mucciarelli, A., Carretta, E., Origlia, L., & Ferraro, F. R. 2008, AJ, 136, 375

Mucciarelli, A., Cristallo, S., Brocato, E., Pasquini, L., Straniero, O., Caffau, E., Raimondo, G., Kaufer, A., Musella, I., Ripepi, V., Romaniello, M., & Walker, A. R. 2010, ArXiv e-prints

Mucciarelli, A., Ferraro, F. R., Origlia, L., & Fusi Pecci, F. 2007, AJ, 133, 2053

Olsen, K. A. G., Hodge, P. W., Mateo, M., Olszewski, E. W., Schommer, R. A., Suntzeff, N. B., & Walker, A. R. 1998, MNRAS, 300, 665

Olszewski, E. W., Schommer, R. A., Suntzeff, N. B., & Harris, H. C. 1991, AJ, 101, 515

Pessev, P. M., Goudfrooij, P., Puzia, T. H., & Chandar, R. 2008, MNRAS, 385, 1535

Pietrinferni, A., Cassisi, S., Salaris, M., & Castelli, F. 2004, ApJ, 612, 168

—. 2006, ApJ, 642, 797

Piotto, G., De Angeli, F., King, I. R., Djorgovski, S. G., Bono, G., Cassisi, S., Meylan, G., Recio-Blanco, A., Rich, R. M., & Davies, M. B. 2004, ApJ, 604, L109

Piotto, G., King, I. R., Djorgovski, S. G., Sosin, C., Zoccali, M., Saviane, I., De Angeli, F., Riello, M., Recio-Blanco, A., Rich, R. M., Meylan, G., & Renzini, A. 2002, A&A, 391, 945

Pritzl, B. J., Venn, K. A., & Irwin, M. 2005, AJ, 130, 2140

Puzia, T. H., Saglia, R. P., Kissler-Patig, M., Maraston, C., Greggio, L., Renzini, A., & Ortolani, S. 2002, A&A, 395, 45

Salaris, M., Chieffi, A., & Straniero, O. 1993, ApJ, 414, 580

Sarajedini, A., Bedin, L. R., Chaboyer, B., Dotter, A., Siegel, M., Anderson, J., Aparicio, A., King, I., Majewski, S., Marín-Franch, A., Piotto, G., Reid, I. N., & Rosenberg, A. 2007, AJ, 133, 1658

Schiavon, R. P. 2007, ApJS, 171, 146

Sneden, C. 1973, ApJ, 184, 839

Testa, V., Ferraro, F. R., Chieffi, A., Straniero, O., Limongi, M., & Fusi Pecci, F. 1999, AJ, 118, 2839

Vazdekis, A., Sánchez-Blázquez, P., Falcón-Barroso, J., Cenarro, A. J., Beasley, M. A., Cardiel, N., Gorgas, J., & Peletier, R. F. 2010, MNRAS, 404, 1639

Vesperini, E., McMillan, S. L. W., & Portegies Zwart, S. 2009, ApJ, 698, 615

Walker, A. R., Raimondo, G., Di Carlo, E., Brocato, E., Castellani, V., & Hill, V. 2001, ApJ, 560, L139

Wolf, M. J., Drory, N., Gebhardt, K., & Hill, G. J. 2007, ApJ,
    655, 179

COLUCCI ET AL.

Table 8
Line Parameters and Integrated Light Equivalent Widths for LMC GCs

Species	λ (Å)	E.P. (eV)	log gf	EW (mÅ) 1916	EW (mÅ) 2005	EW (mÅ) 2019	EW (mÅ) 1978	EW (mÅ) 1718	EW (mÅ) 1866	EW (mÅ) 1711	EW (mÅ) 2100	EW (mÅ) 2002
Fe I	4005.254	1.557	-0.583	⋯	⋯	⋯	⋯	⋯	78.6	⋯	⋯	⋯
Fe I	4076.637	3.211	-0.528	⋯	⋯	⋯	⋯	⋯	41.8	⋯	⋯	⋯
Fe I	4132.067	1.608	-0.675	⋯	⋯	⋯	⋯	⋯	76.8	⋯	⋯	⋯
Fe I	4187.047	2.449	-0.514	⋯	⋯	⋯	⋯	⋯	48.7	⋯	⋯	⋯
Fe I	4199.105	3.047	0.156	85.1	⋯	⋯	⋯	⋯	⋯	⋯	⋯	⋯
Fe I	4206.702	0.052	-3.960	65.6	⋯	⋯	⋯	⋯	⋯	⋯	⋯	⋯
Fe I	4250.130	2.469	-0.380	⋯	⋯	145.7	⋯	⋯	⋯	⋯	⋯	⋯
Fe I	4250.797	1.557	-0.713	133.0	⋯	⋯	⋯	⋯	⋯	⋯	⋯	⋯
Fe I	4282.412	2.176	-0.779	⋯	⋯	96.3	⋯	⋯	⋯	⋯	⋯	⋯
Fe I	4442.349	2.198	-1.228	⋯	⋯	⋯	⋯	⋯	74.9	⋯	⋯	⋯
Fe I	4447.728	2.223	-1.339	⋯	⋯	⋯	⋯	⋯	61.1	⋯	⋯	⋯
Fe I	4461.660	0.087	-3.194	⋯	⋯	128.6	⋯	⋯	⋯	⋯	⋯	⋯
Fe I	4494.573	2.198	-1.143	⋯	⋯	90.7	⋯	98.5	96.8	⋯	⋯	⋯
Fe I	4602.949	1.485	-2.208	⋯	⋯	84.2	157.0	53.4	78.0	⋯	⋯	⋯
Fe I	4632.918	1.608	-2.901	⋯	⋯	⋯	⋯	51.7	⋯	⋯	⋯	⋯
Fe I	4654.504	1.557	-2.721	⋯	⋯	⋯	⋯	63.3	⋯	⋯	⋯	⋯
Fe I	4691.420	2.990	-1.523	⋯	⋯	⋯	⋯	54.1	⋯	⋯	⋯	⋯
Fe I	4736.783	3.211	-0.752	⋯	⋯	⋯	⋯	74.0	83.4	⋯	⋯	107.8
Fe I	4871.325	2.865	-0.362	⋯	128.9	⋯	⋯	⋯	⋯	⋯	⋯	⋯
Fe I	4872.144	2.882	-0.567	121.0	77.7	⋯	⋯	107.1	⋯	⋯	⋯	⋯
Fe I	4890.763	2.875	-0.394	107.8	84.9	84.8	⋯	125.7	⋯	⋯	⋯	⋯
Fe I	4891.502	2.851	-0.111	⋯	131.6	127.6	⋯	⋯	⋯	⋯	⋯	⋯
Fe I	4903.316	2.882	-0.926	83.4	84.9	⋯	⋯	⋯	62.5	⋯	⋯	128.4
Fe I	4918.998	2.865	-0.342	98.4	⋯	⋯	138.9	⋯	⋯	⋯	⋯	⋯
Fe I	4920.514	2.832	0.068	⋯	⋯	155.7	⋯	⋯	⋯	⋯	⋯	⋯
Fe I	4938.820	2.875	-1.077	⋯	⋯	⋯	152.0	64.2	⋯	⋯	⋯	⋯
Fe I	4939.694	0.859	-3.252	78.9	⋯	⋯	⋯	90.7	⋯	⋯	68.9	⋯
Fe I	4966.095	3.332	-0.871	⋯	⋯	⋯	⋯	57.2	⋯	⋯	⋯	136.4
Fe I	4994.138	0.915	-2.969	⋯	68.4	⋯	⋯	⋯	77.3	⋯	⋯	⋯
Fe I	5001.870	3.881	0.050	⋯	⋯	⋯	100.1	⋯	65.1	⋯	⋯	⋯
Fe I	5006.120	2.832	-0.615	⋯	108.4	⋯	⋯	⋯	⋯	⋯	⋯	⋯
Fe I	5014.951	3.943	-0.303	50.0	74.8	⋯	⋯	70.9	⋯	⋯	⋯	⋯
Fe I	5041.763	1.485	-2.203	⋯	⋯	104.8	⋯	⋯	⋯	⋯	⋯	⋯
Fe I	5049.827	2.279	-1.355	93.6	79.6	91.4	⋯	121.0	⋯	⋯	⋯	140.6
Fe I	5051.640	0.915	-2.764	80.3	⋯	105.7	153.3	122.4	85.4	⋯	89.7	⋯
Fe I	5051.640	0.915	-2.764	103.6	⋯	⋯	⋯	⋯	⋯	⋯	⋯	⋯
Fe I	5068.771	2.940	-1.041	⋯	⋯	⋯	⋯	⋯	80.9	⋯	⋯	⋯
Fe I	5074.753	4.220	-0.160	57.1	⋯	⋯	95.4	⋯	61.0	⋯	⋯	73.7
Fe I	5079.745	0.990	-3.245	⋯	⋯	⋯	⋯	84.1	⋯	⋯	⋯	⋯
Fe I	5083.345	0.958	-2.842	⋯	74.4	⋯	⋯	⋯	⋯	⋯	⋯	⋯
Fe I	5123.730	1.011	-3.058	⋯	⋯	⋯	125.5	⋯	⋯	⋯	⋯	⋯
Fe I	5127.368	0.915	-3.249	⋯	⋯	73.9	⋯	⋯	⋯	47.7	⋯	⋯
Fe I	5150.852	0.990	-3.037	⋯	⋯	87.4	110.2	93.2	⋯	⋯	87.3	⋯
Fe I	5151.917	1.011	-3.321	⋯	⋯	⋯	150.9	⋯	⋯	⋯	⋯	⋯
Fe I	5162.281	4.178	0.020	52.8	⋯	⋯	113.6	142.3	⋯	⋯	⋯	⋯
Fe I	5166.284	0.000	-4.123	⋯	⋯	103.3	⋯	107.0	⋯	⋯	⋯	⋯
Fe I	5171.610	0.000	-1.721	⋯	⋯	⋯	151.9	⋯	⋯	⋯	⋯	⋯
Fe I	5191.465	3.038	-0.551	100.2	⋯	95.3	⋯	128.1	⋯	⋯	⋯	⋯
Fe I	5192.353	2.998	-0.421	118.3	⋯	⋯	⋯	133.4	⋯	⋯	⋯	⋯
Fe I	5194.949	1.557	-2.021	⋯	⋯	⋯	151.3	⋯	⋯	61.8	94.9	⋯
Fe I	5195.480	4.220	-0.002	⋯	⋯	⋯	136.5	⋯	⋯	⋯	⋯	⋯
Fe I	5216.283	1.608	-2.082	86.3	⋯	91.9	⋯	69.8	⋯	⋯	⋯	⋯
Fe I	5232.952	2.940	-0.057	114.3	⋯	118.9	⋯	149.9	⋯	⋯	⋯	⋯
Fe I	5254.953	0.110	-4.764	⋯	68.0	⋯	127.2	⋯	⋯	55.2	⋯	⋯
Fe I	5266.563	2.998	-0.385	⋯	96.0	106.3	⋯	⋯	⋯	⋯	⋯	⋯
Fe I	5281.798	3.038	-0.833	⋯	75.9	⋯	101.2	98.1	⋯	43.0	⋯	⋯
Fe I	5283.629	3.241	-0.524	110.5	⋯	⋯	152.9	97.4	⋯	⋯	⋯	⋯
Fe I	5302.307	3.283	-0.720	⋯	⋯	69.5	⋯	124.3	⋯	⋯	⋯	⋯
Fe I	5307.369	1.608	-2.912	62.2	⋯	57.8	90.4	72.5	53.0	⋯	⋯	⋯
Fe I	5324.191	3.211	-0.103	110.2	119.4	102.6	⋯	⋯	85.0	⋯	⋯	⋯
Fe I	5339.937	3.266	-0.720	⋯	69.2	63.8	145.0	61.3	90.7	⋯	⋯	⋯
Fe I	5367.476	4.415	0.443	⋯	⋯	⋯	102.6	⋯	⋯	⋯	⋯	104.7
Fe I	5367.476	4.415	0.443	⋯	⋯	⋯	123.2	⋯	⋯	⋯	⋯	⋯
Fe I	5369.974	4.371	0.536	⋯	⋯	⋯	124.8	101.8	⋯	57.2	⋯	⋯
Fe I	5369.974	4.371	0.536	⋯	⋯	⋯	136.5	⋯	⋯	⋯	⋯	⋯
Fe I	5371.501	0.958	-1.644	⋯	⋯	168.6	⋯	150.7	⋯	73.7	⋯	⋯
Fe I	5383.380	4.312	0.645	70.6	97.1	87.2	⋯	93.6	⋯	43.2	⋯	135.8
Fe I	5389.486	4.415	-0.410	34.9	⋯	⋯	85.7	⋯	⋯	⋯	⋯	⋯
Fe I	5393.176	3.241	-0.715	82.3	63.5	71.6	133.2	114.9	⋯	⋯	⋯	⋯
Fe I	5397.141	0.915	-1.982	⋯	⋯	136.7	⋯	153.7	⋯	45.6	⋯	⋯
Fe I	5405.785	0.990	-1.852	⋯	⋯	139.0	⋯	⋯	⋯	⋯	⋯	⋯
Fe I	5424.080	4.320	0.520	76.8	⋯	⋯	145.2	⋯	⋯	⋯	⋯	⋯
Fe I	5434.534	1.011	-2.126	⋯	69.0	121.2	⋯	116.2	⋯	⋯	⋯	⋯

Table 8 — *Continued*

Species	λ (Å)	E.P. (eV)	log gf	EW (mÅ) 1916	EW (mÅ) 2005	EW (mÅ) 2019	EW (mÅ) 1978	EW (mÅ) 1718	EW (mÅ) 1866	EW (mÅ) 1711	EW (mÅ) 2100	EW (mÅ) 2002
Fe I	5446.924	0.990	-3.109	···	155.9	···	···	···	···	67.4	···	···
Fe I	5455.624	0.000	-2.091	···	···	155.9	···	···	···	···	···	···
Fe I	5455.624	0.000	-2.091	···	···	169.5	···	···	···	···	···	···
Fe I	5497.526	1.011	-2.825	···	93.0	102.4	119.2	123.7	···	···	···	···
Fe I	5501.477	0.958	-3.046	109.8	···	116.9	118.6	89.9	85.9	···	···	···
Fe I	5506.791	0.990	-2.789	142.4	108.7	112.3	···	83.7	103.6	···	···	···
Fe I	5569.631	3.417	-0.500	75.9	···	65.8	···	123.0	···	···	71.0	155.3
Fe I	5572.851	3.396	-0.275	···	···	···	···	···	106.5	···	···	···
Fe I	5576.099	3.430	-0.900	···	···	46.6	···	···	72.7	···	···	125.3
Fe I	5586.771	4.260	-0.096	···	···	···	···	155.3	···	···	···	157.4
Fe I	5586.771	4.260	-0.096	···	···	···	···	127.1	···	···	···	···
Fe I	5763.002	4.209	-0.450	···	···	57.9	87.1	81.1	···	···	···	122.2
Fe I	6136.624	2.453	-1.410	129.1	106.6	···	129.7	···	···	···	···	···
Fe I	6137.702	2.588	-1.346	108.7	···	85.9	126.3	···	···	71.6	···	···
Fe I	6151.623	2.180	-3.330	···	···	···	···	···	112.7	···	···	···
Fe I	6173.341	2.220	-2.863	40.0	···	···	···	62.5	49.1	···	···	···
Fe I	6180.209	2.730	-2.628	···	···	···	···	61.2	47.8	···	···	···
Fe I	6187.995	3.940	-1.673	···	···	···	···	···	33.1	···	···	···
Fe I	6200.321	2.610	-2.386	56.2	52.3	···	···	72.3	49.1	···	88.4	105.4
Fe I	6213.437	2.220	-2.490	···	54.7	···	···	89.2	···	···	···	···
Fe I	6219.287	2.200	-2.428	76.6	56.5	···	126.3	73.5	64.3	···	93.3	152.4
Fe I	6229.232	2.830	-2.821	31.5	···	···	···	···	···	···	···	82.9
Fe I	6230.736	2.559	-1.276	101.3	···	···	···	···	75.6	···	···	···
Fe I	6246.327	3.600	-0.796	···	···	···	141.4	65.0	59.6	···	67.9	···
Fe I	6252.565	2.404	-1.767	71.9	···	···	132.1	116.5	101.5	···	···	···
Fe I	6254.253	2.280	-2.435	55.6	···	60.5	96.3	72.3	···	···	···	···
Fe I	6265.141	2.180	-2.532	···	···	···	···	86.3	···	···	87.5	···
Fe I	6311.504	2.830	-3.153	···	···	···	···	···	54.7	···	···	···
Fe I	6322.694	2.590	-2.438	···	36.3	47.7	128.7	···	58.9	47.4	63.4	···
Fe I	6330.852	4.730	-1.640	···	···	···	···	···	23.7	···	···	33.0
Fe I	6335.337	2.200	-2.175	74.2	58.6	67.4	135.6	74.1	67.3	53.5	···	···
Fe I	6336.830	3.690	-0.667	59.5	···	···	134.6	65.8	68.7	40.4	···	···
Fe I	6353.849	0.910	-6.360	···	···	···	···	···	86.5	···	···	···
Fe I	6355.035	2.840	-2.328	60.7	···	49.6	···	68.0	46.5	···	93.1	···
Fe I	6380.750	4.190	-1.366	···	···	···	···	···	42.7	···	···	···
Fe I	6392.538	2.280	-3.957	···	···	···	···	30.2	···	···	···	···
Fe I	6393.612	2.430	-1.505	95.0	···	91.7	···	129.9	93.9	···	···	···
Fe I	6400.009	3.602	-0.290	···	···	···	···	143.3	···	69.3	···	···
Fe I	6411.658	3.650	-0.646	73.2	79.8	67.9	100.4	···	78.9	···	···	158.7
Fe I	6419.956	4.730	-0.183	···	···	···	···	···	56.0	···	···	···
Fe I	6421.360	2.280	-1.979	83.9	90.2	88.0	142.5	92.0	80.7	···	···	···
Fe I	6430.856	2.180	-1.954	···	74.3	76.7	···	118.9	···	···	···	···
Fe I	6475.632	2.560	-2.929	···	···	36.7	97.9	40.9	···	···	84.5	···
Fe I	6481.878	2.280	-2.985	···	···	···	100.1	···	···	···	···	···
Fe I	6494.994	2.400	-1.246	103.3	87.8	124.5	···	143.7	···	···	···	···
Fe I	6498.945	0.960	-4.675	···	···	···	86.0	···	···	···	···	···
Fe I	6518.373	2.830	-2.397	···	···	···	···	···	96.5	···	···	132.9
Fe I	6533.940	4.540	-1.360	···	···	···	58.3	···	···	···	48.1	36.4
Fe I	6546.252	2.750	-1.536	···	···	···	···	143.1	···	···	95.2	134.0
Fe I	6593.874	2.430	-2.377	···	58.4	···	···	···	···	···	···	···
Fe I	6597.571	4.770	-0.970	···	···	···	···	···	37.5	···	···	···
Fe I	6608.044	2.270	-3.939	···	···	···	···	44.9	···	···	64.5	···
Fe I	6646.966	2.600	-3.917	···	···	···	···	···	54.1	···	···	52.3
Fe I	6648.121	1.010	-5.730	···	···	···	···	···	77.8	···	···	107.0
Fe I	6677.997	2.690	-1.395	93.9	···	91.4	···	103.3	111.0	···	···	···
Fe I	6703.576	2.760	-3.059	31.5	···	23.6	79.0	40.1	37.6	···	57.4	···
Fe I	6705.105	4.610	-1.060	···	···	···	···	34.0	35.7	···	52.0	···
Fe I	6710.323	1.480	-4.807	···	···	···	···	···	88.7	···	···	···
Fe I	6725.364	4.100	-2.227	···	···	···	···	···	60.7	···	···	···
Fe I	6739.524	1.560	-4.801	···	···	···	67.4	44.9	···	···	···	···
Fe I	6750.164	2.420	-2.592	···	···	···	···	66.0	44.8	···	90.2	151.1
Fe I	6752.716	4.640	-1.263	···	···	···	···	···	70.8	···	···	···
Fe I	6806.856	2.730	-2.633	27.1	···	···	···	38.7	48.8	···	70.5	91.3
Fe I	6810.267	4.590	-0.992	···	···	···	···	···	64.3	···	···	67.6
Fe I	6828.596	4.640	-0.843	···	···	···	···	···	47.9	···	···	82.3
Fe I	6839.835	2.560	-3.378	···	···	···	77.4	56.5	33.3	···	58.3	100.0
Fe I	6841.341	4.610	-0.733	39.3	···	···	···	72.7	50.5	···	53.5	83.7
Fe I	6842.689	4.640	-1.224	···	···	···	···	···	32.4	···	···	50.2
Fe I	6843.655	3.650	-0.863	···	···	···	···	···	51.6	···	···	52.6
Fe I	6851.652	1.600	-5.247	···	···	···	···	···	51.0	···	···	73.4
Fe I	6855.723	4.390	-1.747	···	···	···	···	···	34.0	···	···	···
Fe I	6916.686	4.150	-1.359	···	···	···	···	···	133.7	···	···	···
Fe I	6960.330	4.570	-1.907	···	···	···	···	···	37.8	···	···	···
Fe I	7007.976	4.180	-1.929	···	···	···	···	···	105.2	···	···	···

COLUCCI ET AL.

Table 8 — *Continued*

Species	λ (Å)	E.P. (eV)	log gf	EW (mÅ) 1916	EW (mÅ) 2005	EW (mÅ) 2019	EW (mÅ) 1978	EW (mÅ) 1718	EW (mÅ) 1866	EW (mÅ) 1711	EW (mÅ) 2100	EW (mÅ) 2002
Fe I	7022.957	4.190	-1.148	⋯	⋯	⋯	⋯	⋯	134.8	⋯	⋯	⋯
Fe I	7038.220	4.220	-1.214	⋯	⋯	⋯	⋯	65.5	⋯	⋯	⋯	139.6
Fe I	7068.423	4.070	-1.319	⋯	⋯	26.3	⋯	⋯	⋯	48.7	⋯	143.1
Fe I	7071.866	4.610	-1.627	⋯	⋯	⋯	⋯	⋯	34.9	⋯	⋯	⋯
Fe I	7072.800	4.070	-2.767	⋯	⋯	⋯	⋯	⋯	23.0	⋯	⋯	⋯
Fe I	7090.390	4.230	-1.109	⋯	⋯	⋯	⋯	⋯	135.1	⋯	⋯	⋯
Fe I	7127.573	4.990	-1.177	⋯	⋯	⋯	⋯	⋯	55.7	⋯	⋯	⋯
Fe I	7130.925	4.300	-0.708	⋯	⋯	⋯	⋯	91.7	70.5	⋯	⋯	146.2
Fe I	7132.985	4.060	-1.635	⋯	⋯	⋯	⋯	64.0	39.1	⋯	⋯	94.2
Fe I	7142.517	4.930	-1.017	⋯	⋯	⋯	⋯	⋯	41.7	⋯	⋯	⋯
Fe I	7145.312	4.610	-1.240	⋯	⋯	⋯	⋯	41.5	⋯	⋯	⋯	80.1
Fe I	7151.464	2.480	-3.657	⋯	⋯	⋯	⋯	⋯	45.6	⋯	⋯	123.0
Fe I	7155.634	4.990	-1.017	⋯	⋯	⋯	⋯	⋯	81.4	⋯	⋯	⋯
Fe I	7411.162	4.280	-0.287	73.6	⋯	⋯	⋯	⋯	100.7	⋯	⋯	⋯
Fe I	7445.758	4.260	0.053	82.3	69.4	⋯	⋯	99.8	115.1	89.5	⋯	⋯
Fe I	7454.004	4.190	-2.337	⋯	⋯	⋯	⋯	⋯	47.1	⋯	⋯	⋯
Fe I	7461.527	2.560	-3.507	⋯	⋯	⋯	⋯	⋯	62.3	⋯	⋯	⋯
Fe I	7491.652	4.280	-1.067	⋯	⋯	⋯	⋯	89.4	⋯	⋯	⋯	⋯
Fe I	7507.273	4.410	-1.107	⋯	⋯	⋯	⋯	49.7	64.7	⋯	⋯	⋯
Fe I	7531.153	4.370	-0.557	⋯	⋯	⋯	⋯	86.6	⋯	71.4	⋯	⋯
Fe I	7540.444	2.730	-3.777	⋯	⋯	⋯	60.2	⋯	⋯	⋯	70.0	124.2
Fe I	7583.790	3.018	-1.885	⋯	⋯	57.2	⋯	⋯	⋯	58.8	⋯	⋯

Note. — Lines listed twice correspond to those measured in adjacent orders with overlapping wavelength coverage.